Lattice dependence of saturated ferromagnetism in the Hubbard model

Thoralf Hanisch, Götz S. Uhrig, and Erwin Müller-Hartmann
Institut für Theoretische Physik, Universität zu Köln, D-50937 Köln, Germany
(Received 10 July 1997)

We investigate the instability of the saturated ferromagnetic ground state (Nagaoka state) in the Hubbard model on various lattices in dimensions $d=2$ and $d=3$. A variational resolvent approach is developed for the Nagaoka instability both for $U=\infty$ and for $U<\infty$ which can easily be evaluated in the thermodynamic limit on all common lattices. Our results significantly improve former variational bounds for a possible Nagaoka regime in the ground-state phase diagram of the Hubbard model. We show that a pronounced particle-hole asymmetry in the density of states and a diverging density of states at the lower band edge are the most important features in order to stabilize Nagaoka ferromagnetism, particularly in the low-density limit. [S0163-1829(97)08345-8]

I. INTRODUCTION

It is by now an often repeated fact that the so-called (single-band) Hubbard model was originally introduced to explain ferromagnetism.[1–3] In what followed, however, it turned out to be rather a generic model for antiferromagnetism. Ferromagnetism seemed to require additional ingredients, for instance, the existence of degenerate bands which favor ferromagnetism based on Hund's rule or in the insulating case certain additional ferromagnetic couplings and/or correlated hopping terms. Both scenarios were proven rigorously in recent years (see Ref. 4 and references therein for the former and Ref. 5 and references therein for the latter).

The Hubbard model and its possible ferromagnetic ground state are of renewed interest.[6,7] There are many works in the field based on quasi-one-dimensional ($d=1$) systems triggered by the prediction of ferromagnetism in double minima systems at low particle density[8] and by the numerous possibilities of analytical and numerical calculations[9–12] in $d=1$. Exact calculations are possible in infinite dimensions ($d=\infty$).[13,14] For intermediate dimensions ($1<d<\infty$) numerical and approximate methods are employed.[15–17]

An important milestone in the research of ferromagnetism in Hubbard models is the work of Nagaoka.[18,19] It showed that at infinite local repulsion a single electron above half filling favors the saturated ferromagnetic ground state (henceforth: Nagaoka state) if the underlying lattice has loops which allow interference. For bipartite lattices particle-hole symmetry extends these results to hole doping. This result reveals the beauty and the difficulty of the question for which lattices and for which fillings the Nagaoka state is the ground state. At $U=\infty, T=0$ there is only the hopping left as a global energy scale. Thus there is no expansion parameter, no adiabatic limit, and no competition of energy scales. The issue is solely a question of the lattice structure, i.e., the possible paths on the lattice, and of the filling.

Unfortunately, there are no extensions of Nagaoka's result to macroscopic dopings. Only nonmacroscopic numbers of holes could be treated.[20,21] Therefore, we choose another route in the present work and investigate the stability of the Nagaoka state towards a single spin flip. If such a flip lowers the energy then the Nagaoka state is not the ground state. Otherwise it is locally stable. The drawback that we treat only local stability in this way is not very serious. There is no indication that the transition away from saturation should not be continuous at $T=0$, see e.g., Ref. 22.

A more serious drawback is the fact that even the single spin flip is too difficult a problem to be solved completely on finite-dimensional lattices. In the limit of infinite dimensional lattices, however, it was solved.[13] Thereby it was shown that relatively simple variational ansatzes provide already a qualitative insight in the tendency of a certain lattice to have a Nagaoka state as ground state. Wurth *et al.* showed that only an extremely sophisticated variational ansatz[23] yields a further reduction of the region of possible Nagaoka state stability in comparison to simpler ansatzes.[24]

It is the aim of the present paper to extend previous work on variational ansatzes decisively,[25] both in the completeness of the ansatzes and in the types of the lattices considered. So far, variational ansatzes considered a finite vicinity of the flipped spin and treated a finite number of parameters leading to matrix eigenvalue problems. Here we will show that a resolvent approach is capable to deal implicitly with an *infinite* number of variational parameters. No explicit knowledge of the variational wave function is required. A similar approach was used recently by Okabe[26] for the square lattice and the simple cubic lattice, too. In his work, however, the reduction of the resolvent to simple integrals over the density of states (DOS), which we succeeded to achieve in most cases, is lacking.

We will present elegant simple expressions for the Nagaoka instability line $U_{\mathrm{cr}}(n)$ which apply to most common lattices. These results make it possible for everyone to check easily whether or not one can expect a ferromagnetic ground state for a given lattice. We will show that two main features favor the occurrence of a saturated ferromagnetic ground state:

(1) A highly asymmetric density of states with large values at the lower band edge (after particle-hole transformation).

(2) Nonbipartiteness of the lattice, i.e., frustration due to loops of three sites.

Of course, the two points are intimately related.

The setup of our article is as follows. In the rest of the Introduction we will present certain variational ansatzes used

so far to investigate the Nagaoka state stability. In Sec. II we develop the resolvent approach which yields simple formulas for the stability lines on homogeneous, isotropic lattices with nearest-neighbor hopping. In Sec. III we present our results for various lattices in dimensions $d=2$ and $d=3$, namely the square, the simple cubic, the bcc, the honeycomb, the triangular, the *kagomé*, and the fcc (hcp) lattice. For the t-$t\prime$ Hubbard model on the square lattice a perturbative approach for small $|t|$ is employed as well. Section IV contains a summary and a final discussion of the lattice dependence of saturated ferromagnetism in the Hubbard model. The appendixes contain technical details in the derivation for the various lattices.

Preliminary approaches

We consider the conventional single-band Hubbard model

$$H=-t\sum_{\langle \underline{i},\underline{j}\rangle\sigma} a^{+}_{\underline{i}\sigma}a_{\underline{j}\sigma}+U\sum_{\underline{i}} a^{+}_{\underline{i}\uparrow}a_{\underline{i}\uparrow}a^{+}_{\underline{i}\downarrow}a_{\underline{i}\downarrow} \tag{1}$$

and calculate the spin-flip energy

$$\Delta e=\langle\Psi|H-E_{\mathcal{N}}|\Psi\rangle/\langle\Psi|\Psi\rangle, \tag{2}$$

where $E_{\mathcal{N}}$ is the energy of the Nagaoka state and $|\Psi\rangle$ is a variational wave function. Whenever $\Delta e<0$ the Nagaoka state is definitely not the ground state due to the variational nature of our approach. At $U=\infty$, the zero of $\Delta e_{\infty}(\delta):=\Delta e(U=\infty,\delta)$ gives the critical hole density δ_{cr} above which the Nagaoka state is unstable. For finite U, $\Delta e(U,\delta)\doteq 0$ leads to the Nagaoka instability line $U_{\mathrm{cr}}(\delta)$ which separates a region of guaranteed instability of the Nagaoka state $[U<U_{\mathrm{cr}}(\delta)]$ in the phase diagram of the Hubbard model from a region of possible stability of the Nagaoka state $[U>U_{\mathrm{cr}}(\delta)]$. In the phase diagrams displayed in this paper we will always represent the on-site repulsion U in terms of $U_{\mathrm{red}}=U/(U+U_{\mathrm{BR}})$ where $U_{\mathrm{BR}}=-16\epsilon^{0}$ denotes the Brinkman-Rice critical coupling.[27] ϵ^{0} is the energy per particle of the saturated ferromagnetic state for the quarter-filled band and depends on the underlying lattice. This representation is chosen to render comparisons between different lattices possible.

A common starting point[28–30,24,25] is defined by the ansatz

$$|\Psi\rangle:=|\Lambda|^{-1/2}\sum_{\underline{i}}\exp(i\underline{k}_{\mathrm{b}}\underline{i})\left[a_{\underline{i}\uparrow}\left(a^{+}_{\underline{i}\uparrow}+f\cdot\sum_{\langle\underline{i},\underline{j}\rangle}a^{+}_{\underline{j}\uparrow}\right)+g\cdot a^{+}_{\underline{i}\uparrow}a_{\underline{i}\uparrow}\right]a^{+}_{\underline{i}\downarrow}|\mathcal{N}\rangle. \tag{3}$$

For $f=0$ this is the Gutzwiller single spin-flip wave function (Gw). The parameter g controls the probability of double occupancy. The system size is denoted by $|\Lambda|$. We use the operators $a(a^{+})$ for site-diagonal fermion annihilation (creation) and $c(c^{+})$ for momentum diagonal fermion annihilation (creation). Furthermore, we use n for the particle density, $\delta=1-n$ for the doping per site, z for the coordination number, and $e_1=E_{\mathcal{N}}/|\Lambda|$ for the expectation value of the kinetic energy. The ket $|\mathcal{N}\rangle=c_{\underline{k}_{\mathrm{F}}\uparrow}|\mathcal{N}\rangle$ is the fully polarized Fermi sea of $\uparrow$ electrons from which one $e^{-}_{\uparrow}$ at the Fermi level ε_{F} is removed. The energy balance of Eq. (3) with $f=0$ reads at infinite U $(g=0)$ (see Refs. 28 and 24)

$$\Delta e=-e_1/\delta-\varepsilon_{\mathrm{F}}+\varepsilon_{\underline{k}}\delta[1-(e_1/\delta zt)^2], \tag{4}$$

where ε_k is the dispersion. The maximum energy lowering is obviously obtained for $\underline{k}$ belonging to the lower band egde ε_{b}, i.e., here $\underline{k}_{\mathrm{b}}=\underline{0}$.

For finite f majority-spin hopping processes from the position of the flipped spin to nearest-neighbor sites are taken into account. This ansatz will be denoted NN. The amplitudes of these hopping processes are assumed to reflect the lattice symmetry. Basile and Elser investigated an ansatz similar to NN which includes $\uparrow$-hopping processes from the position of the $\downarrow$ electron to *all* other lattice sites.[31] Since the number of variational parameters increases with the lattice size they only studied a finite square lattice. The resolvent method developed in Sec. II allows us to investigate a variational ansatz equivalent to the full Basile-Elser wave function *in the thermodynamic limit* on all common lattices. We also derive improved variational criteria for the Nagaoka instability at $U<\infty$ by extending the Hilbert subspace further.

II. RESOLVENT APPROACH

Generally, a resolvent is an operator-valued expression of the type

$$R(\omega)=1/[\omega-(H-E_{\mathcal{N}})], \tag{5}$$

where $H-E_{\mathcal{N}}$ is the Hamilton operator with respect to the ground-state energy $E_{\mathcal{N}}$ (here: the Nagaoka state energy). From Eq. (5) it is clear that the existence of any state at $\omega=\omega_0$ implies a pole or at least a singularity in the resolvent. For this reason, we will investigate in the following the resolvent R applied to $c^{+}_{\underline{k}_{\mathrm{b}}\downarrow}|\mathcal{N}\rangle$ and compare ω_0 to ε_{F}.

It is not possible to compute R for the whole Hilbert space except under simplifying conditions like infinite coordination number.[32] Hence we will restrict the inversion to certain subspaces which still allow an analytical treatment. The results obtained in this way for the lower band edge are variational. This means that excitation energies found are upper bounds to the true ones and that specific interaction values U come out too small compared to those of the full solution.

A. Case $U=\infty$: Ansatz RES0

For infinite on-site repulsion no double occupancy is allowed. Thus at the site of the $\downarrow$-e^{-} no $\uparrow$-e^{-} is allowed. We investigate therefore the variational subspace spanned by $a_{\underline{i}\uparrow}a^{+}_{\underline{j}\uparrow}a^{+}_{\underline{i}\downarrow}|\mathcal{N}\rangle$ with arbitrary $\underline{i}$ and

NN ansatz (3) and of course the simple Gutzwiller ansatz. It comprises $\uparrow$-hopping processes of arbitrary distance, i.e., it is the thermodynamic extension of the ansatz investigated previously by Basile and Elser.[31]

For the computation of the resolvent $R(\omega)$ one can use the Mori/Zwanzig projection formalism (see, e.g., Appendix C in Ref. 33) with the scalar product $(\mathcal{A}|\mathcal{B}) := \langle \mathcal{N}| [\mathcal{A}^+, \mathcal{B}]_+ |\mathcal{N}\rangle$ for the operators $\mathcal{A}$ and $\mathcal{B}$. The resolvent (5) then becomes

$$\mathbf{R}_{\underline{k}_1,\underline{k}_2}(\omega) = \langle \Phi_{\underline{k}_1} | R(\omega) | \Phi_{\underline{k}_2} \rangle = (\mathcal{A}_{\underline{k}_1} | (\omega - \mathcal{L})^{-1} \mathcal{A}_{\underline{k}_2}). \tag{7}$$

Here the Liouville operator $\mathcal{L}$ is used which is defined as $\mathcal{L}\mathcal{A} := [H, \mathcal{A}]$ for all operators $\mathcal{A}$.[33] The resolvent can be expressed in matrix notation[33] by

$$\mathbf{R}(\omega) = \mathbf{P}[\omega \mathbf{P} - \mathbf{L} - \mathbf{M}(\omega)]^{-1} \mathbf{P} \tag{8}$$

with the norm matrix $\mathbf{P}$ and the frequency matrix $\mathbf{L}$

$$\mathbf{P}_{\underline{k}_1,\underline{k}_2} := \langle \Phi_{\underline{k}_1} | \Phi_{\underline{k}_2} \rangle, \tag{9a}$$

$$\mathbf{L}_{\underline{k}_1,\underline{k}_2} := \langle \Phi_{\underline{k}_1} | H - E_{\mathcal{N}} | \Phi_{\underline{k}_2} \rangle. \tag{9b}$$

The frequency matrix $\mathbf{L}$ encodes the effect of H in the subspace considered. The deviation of $\mathbf{P}$ from unity accounts for the nonorthonormality of the basis. The so-called memory matrix $\mathbf{M}(\omega)$ describes the effect of all processes which imply excursions outside the subspace considered. If the ground state is known exactly (which holds in the present case) the approximation $\mathbf{M}(\omega) = \mathbf{0}$ is variational in nature for the lower band edge.

It is the aim of the subsequent calculation to obtain a simple condition for the singularity of $(\omega \mathbf{P} - \mathbf{L})$. This singularity then signals that ω corresponds to an eigenenergy. To this end, we first need the matrix elements

$$\mathbf{P}_{\underline{k}_1,\underline{k}_2} = n \delta_{\underline{k}_1,\underline{k}_2} + |\Lambda|^{-1}, \tag{10a}$$

$$\mathbf{L}_{\underline{k}_1,\underline{k}_2\uparrow} = \delta_{\underline{k}_1,\underline{k}_2} (n \cdot \varepsilon_{\underline{k}_2} - e_1), \tag{10b}$$

$$\mathbf{L}_{\underline{k}_1,\underline{k}_2\downarrow} = |\Lambda|^{-1} \varepsilon_{\mathrm{b}} - \delta_{\underline{k}_1,\underline{k}_2} (zt)^{-1} e_1 \varepsilon_{\underline{k}_2 - \underline{k}_{\mathrm{b}}}. \tag{10c}$$

We use the notation $e_i := \langle \Theta(\varepsilon_F - \varepsilon_{\underline{k}}) \varepsilon_{\underline{k}}^i \rangle_{\mathrm{BZ}}$ [$\Theta(\varepsilon)$ is the Heaviside function]. The elements in Eq. (10) are obtained with the help of Wick's theorem since $|\mathcal{N}\rangle$ is a simple Slater determinant. In Eqs. (10b) and (10c), we distinguish the part coming from the motion of the $\uparrow$ electrons and the part coming from the motion of the $\downarrow$ electron. The expression $(zt)^{-1} e_1 \varepsilon_{\underline{k}_2 - \underline{k}_{\mathrm{b}}}$ in Eq. (10c) is obtained from

$$-(2\pi)^{-d} \int_{\underline{k}_1 \in \mathrm{BZ} \setminus \mathrm{FS}} \varepsilon_{\underline{k}_2 - \underline{k}_{\mathrm{b}} - \underline{k}_1} d^d k_1 = \frac{1}{zt} \varepsilon_{\underline{k}_2 - \underline{k}_{\mathrm{b}}} \underbrace{(2\pi)^{-d} \int_{\underline{k}_1 \in \mathrm{BZ} \setminus \mathrm{FS}} \varepsilon_{\underline{k}_1} d^d k_1}_{e_1 :=}. \tag{11}$$

This relation holds for all homogeneous, isotropic lattices with NN hopping only, e.g., square lattice, triangular lattice, *kagomé* lattice, and so on. The result (11) can be found easiest by interpreting the left-hand side as convolution of $\varepsilon_{\underline{k}_2 - \underline{k}_{\mathrm{b}}}$ and of $\Theta(\varepsilon_{\mathrm{F}} - \varepsilon_{\underline{k}_1})$, i.e., as a multiplication in real space which concerns only the NN terms. Thus it is the multiplication with a constant $\langle a_{\underline{j}} a_{\underline{i}}^+ \rangle = -e_1/(zt)$. The sites $\underline{i}$ and $\underline{j}$ are arbitrary adjacent sites since all bonds are equal due to the required homogeneity and spatial isotropy.

On the basis of Eq. (10) the matrix inversion can be rephrased as

$$(\omega \mathbf{P} - \mathbf{L})^{-1} = [\mathbf{d}^{-1} + (\omega - \varepsilon_{\mathrm{b}}) \underline{v}\, \underline{v}^+]^{-1} \tag{12}$$

with the constant vector $\underline{v} = |\Lambda|^{-1/2}$ and the diagonal matrix $\mathbf{d}_{\underline{k}_1 \underline{k}_2} = \delta_{\underline{k}_1 \underline{k}_2} f(\underline{k}_2)$ with

$$f(\underline{k})$$

In Appendix C it is explained that computing $h(\omega)$ for nonbipartite lattices requires explicit integration over the momenta. For lattices where the band minimum ε_b is reached at $\underline{k}_b=\underline{0}$ further simplification is possible. The band minimum is found at $\underline{k}_b=\underline{0}$ in particular for bipartite lattices where one may choose $t>0$ without loss of generality. Then the term $\varepsilon_{\underline{k}-\underline{k}_b}$ in Eq. (13) reduces to the unshifted dispersion and the whole integration in Eq. (14a) can be written as integration over the density of states (DOS) $\rho(\varepsilon)$:

$$h(\omega)=\int_{\varepsilon_F}^{\varepsilon_t}\frac{\rho(\varepsilon)d\varepsilon}{n\omega+e_{\mathcal{N}}-\gamma\varepsilon}=\frac{1}{\gamma}G(\Omega), \tag{16a}$$

$$G(y):=\int_{\varepsilon_F}^{\varepsilon_t}\frac{\rho(\varepsilon)d\varepsilon}{y-\varepsilon}, \tag{16b}$$

$$\gamma:=n-e_1/zt, \tag{16c}$$

$$\Omega:=(n\omega+e_1)/\gamma. \tag{16d}$$

We will call the ansatz deduced from the subspace given in Eq. (6) RES0. It leads to the singularity condition (15) or to its generalizations for non-Bravais lattices.

Once the energy ω is found from Eq. (15) for a given Fermi energy ε_F the spin flip energy for the whole process of taking one $\uparrow$-e^- out at the Fermi level and inserting it as $\downarrow$-e^- at the lowest possible energy is given by

$$\Delta e_\infty=\omega-\varepsilon_F. \tag{17}$$

A critical doping δ_{cr} is found where this spin-flip energy vanishes.

B. Case $U<\infty$: Ansatzes RES1, RES2, and RES3

Besides the calculation of variational upper bounds for spin-flip energies and resulting critical dopings it is our aim to determine critical interaction values U. For $U<\infty$ we have to include states with double occupancy. The easiest way to do so is to include a local double occupancy.[34,28] This is done in the ansatz RES1 by adding to the states defined in Eq. (6) the state

$$|\Psi_1\rangle:=|\Lambda|^{-1/2}\sum_{\underline{i}}\exp(i\underline{k}_b\underline{i})a^+_{\underline{i}\uparrow}a_{\underline{i}\uparrow}a^+_{\underline{i}\downarrow}|\mathcal{N}\mathcal{G}\rangle. \tag{18}$$

This ansatz contains the nearest-neighbor ansatz NN (3) (and the Gutzwiller ansatz) for $U<\infty$. Again we want to compute the resolvent (8). To do so the parts computed in the previous subsection can be used again. The matrices for RES1 have the block structure

$$\mathbf{P}=\begin{pmatrix}\mathbf{P_1} & \underline{0}^+\\ \underline{0} & P_2\end{pmatrix},\quad \omega\mathbf{P}-\mathbf{L}=\begin{pmatrix}\mathbf{D_1} & \underline{N}\\ \underline{N}^+ & D_2\end{pmatrix}, \tag{19a}$$

$$(\omega\mathbf{P}-\mathbf{L})^{-1}=\begin{pmatrix}\mathbf{B_1} & \underline{M}\\ \underline{M}^+ & B_2\end{pmatrix}. \tag{19b}$$

The matrices $\mathbf{P_1}$ and $\mathbf{D_1}$ are the same as in Eq. (14c) at $U=\infty$. The null vector $\underline{0}$ in $\mathbf{P}$ comes from the fact that the state with double occupancy $|\Psi_1\rangle$ is orthogonal to the states without double occupancy $|\Phi_{\underline{k}}\rangle$. The other matrix elements are again found by Wick's theorem

$$P_2=n, \tag{20a}$$

$$D_2=n(\omega-U)+e_1-\varepsilon_b[n^2-(e_1/(zt))^2], \tag{20b}$$

$$N_{\underline{k}}=-|\Lambda|^{-1/2}[n(\varepsilon_b-\varepsilon_{\underline{k}})+e_1(1+\varepsilon_{\underline{k}-\underline{k}_b}/(zt))]. \tag{20c}$$

Since we are at present only interested in the singularity condition it is sufficient to compute one of the elements of $\omega\mathbf{P}-\mathbf{L}$. The easiest is B_2, for which an argument similar to the one leading to Eq. (14b), yields

$$B_2=(D_2-\underline{N}^+\mathbf{D_1}^{-1}\underline{N})^{-1}. \tag{21}$$

Thus the singularity condition simply reads

$$0\doteq D_2-\underline{N}^+\mathbf{D_1}^{-1}\underline{N}. \tag{22}$$

Now it is advantageous that $\mathbf{D_1}^{-1}$ is already given in Eq. (14c). Inserting Eq. (20) one obtains after some cancellations

$$\omega-\varepsilon_b-nU[1+(\omega-\varepsilon_b)h(\omega)]\doteq 0. \tag{23}$$

Equation (23) is as simple as Eq. (15) and enables us to calculate critical U values explicitly. Setting $\omega=\varepsilon_F$ in Eq. (23), which according to Eq. (17) corresponds to vanishing spin-flip energy, renders U_{cr} directly accessible:

$$U_{cr}^{RES1}(\delta)=\frac{\varepsilon_F-\varepsilon_b}{(1-\delta)[1+(\varepsilon_F-\varepsilon_b)h(\varepsilon_F)]}. \tag{24}$$

It turns out, however, that the values for U_{cr} from Eq. (24) are not very good close to half-filling $n=1$ where antiferromagnetic exchange processes are important. These are not accounted for in Eq. (18). They are considered, at least to a certain extent, in the ansatz RES2 by using

$$|\Psi_2\rangle:=|\Lambda|^{-1/2}\sum_{\langle\underline{ij}\rangle}\exp(i\underline{k}_b\underline{i})a^+_{\underline{i}\uparrow}a_{\underline{j}\uparrow}a^+_{\underline{i}\downarrow}|\mathcal{N}\mathcal{G}\rangle, \tag{25}$$

instead of $|\Psi_1\rangle$ as an extension of the RES0 subspace.

The block structure (19) remains the same and so does the singularity condition (22). Only the matrix elements are modified

$$P_2=(e_1^2+\delta e_2)/t^2, \tag{26a}$$

$$D_2=\{(e_1^2+\delta e_2)(\omega-U)+e_1e_2+\delta e_3-\varepsilon_b[e_1^2-e_1e_3/(zt)^2]\}/t^2, \tag{26b}$$

$$N_{\underline{k}}=|\Lambda|^{-1/2}\{e_1(\varepsilon_b-\varepsilon_{\underline{k}})+e_2[1+\varepsilon_{\underline{k}-\underline{k}_b}/(zt)]\}/t. \tag{26c}$$

The explicit expression resulting now from Eq. (22) is less transparent than Eq. (23) since no cancellations occur. We focus here on the most important case $\underline{k}_b=\underline{0}$. In addition to the definitions (16) we use

$$\gamma\mathcal{G}:=e_1-e_2/(zt), \tag{27a}$$

$$\Omega_b:=(e_1\varepsilon_b+e_2)/\gamma\mathcal{G}, \tag{27b}$$

$$y:=(\gamma\delta/\gamma)[\,\delta+(\Omega_{\rm b}-\Omega)G(\Omega)], \tag{27c}$$

and obtain from Eq. (22)

$$D_2 \doteq \sum_{\underline{k}_1,\underline{k}_2\in \mathrm{BZ}\setminus\mathrm{FS}} N^+_{\underline{k}_1}(\mathbf{D_1}^{-1})_{\underline{k}_1,\underline{k}_2}N_{\underline{k}_2}$$
$$= \gamma\delta\left[(\Omega_b-\Omega)y+\frac{\gamma\delta}{\gamma}(\delta\Omega_{\rm b}+e_1)\right]$$
$$-y^2\frac{\omega-\varepsilon_{\rm b}}{1+(\omega-\varepsilon_{\rm b})h(\omega)}, \tag{28}$$

from which $U_{\rm cr}$ can easily be determined. The value $U_{\rm cr}$ appears only in D_2, see Eq. (26b). The results of RES2 (28) generically lead to $U_{\rm cr}\propto 1/\delta$ on vanishing doping. In this sense it represents an important improvement over RES1 (23). For explicit results we refer the reader to the next section.

At last in RES3, we generalize the variational states with double occupancy like Eqs. (18) and (25) in the same manner as we generalized the states without double occupancy in Eq. (6)

$$|\Psi_{\underline{k}}\rangle:=\mathcal{B}_{\underline{k}}|\mathcal{N}\delta\rangle, \tag{29a}$$

$$\mathcal{B}_{\underline{k}}:=|\Lambda|^{-1/2}\sum_{\underline{i}}\exp(i(\underline{k}_{\rm b}+\underline{k})\underline{i})a^+_{\underline{i}\uparrow}c_{\underline{k}\uparrow}a^+_{\underline{i}\downarrow}, \tag{29b}$$

where now the admissible values of $\underline{k}$ are all vectors inside the Fermi sphere (FS). Note that the extension RES3 contains both RES1 and RES2. The block structure of the resulting problem is similar to the one in Eq. (19). The difference is that all blocks are now macroscopically large

$$\mathbf{P}=\begin{pmatrix}\mathbf{P_1} & \mathbf{0}^+\\ \mathbf{0} & \mathbf{P_2}\end{pmatrix},\quad \omega\mathbf{P}-\mathbf{L}=\begin{pmatrix}\mathbf{D_1} & \mathbf{N}\\ \mathbf{N}^+ & \mathbf{D_2}\end{pmatrix}, \tag{30a}$$

$$(\omega\mathbf{P}-\mathbf{L})^{-1}=\begin{pmatrix}\mathbf{B_1} & \mathbf{M}\\ \mathbf{M}^+ & \mathbf{B_2}\end{pmatrix}. \tag{30b}$$

The matrix elements and details of the evaluation are given in Appendix A. The main problem is that one has to find a tractable condition for

$$\mathbf{B_2}^{-1}=\mathbf{D_2}-\mathbf{N}^+\mathbf{D_1}^{-1}\mathbf{N} \tag{31}$$

to be singular. But with expansion tricks similar to the ones used above this obstacle can be overcome. For bipartite lattices a relatively simple final formula is found (A22). An evaluation for the triangular lattice (Appendix C) and the *kagomé* lattice (Appendix D) is possible as well.

III. RESULTS FOR VARIOUS LATTICES

A. Square lattice

The square lattice represents the simplest bipartite lattice structure in two space dimensions and has therefore been at the center of interest in most of the publications dealing with the variational investigation of Nagaoka stability.[23,24,28,31,35–37] The energy band is given by

$$\varepsilon_{\square}(\underline{k})=-2t(\cos k_x+\cos k_y), \tag{32}$$

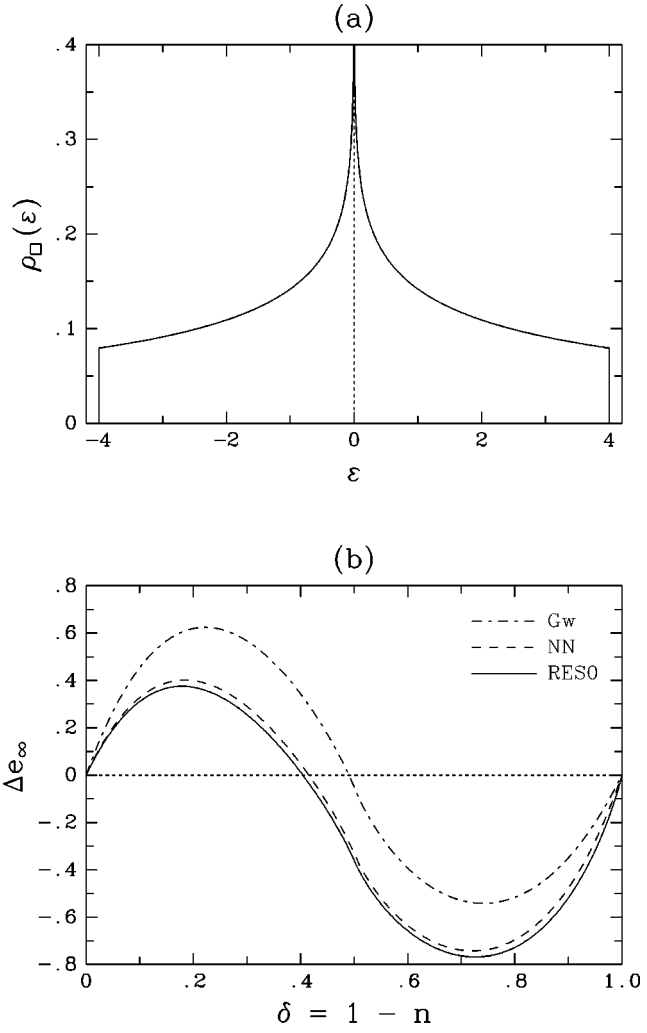

FIG. 1. (a) DOS for the square lattice ($t=1$), (b) spin-flip energy at $U=\infty$ as a function of the hole density for Gw, NN, and RES0 on the square lattice ($t=1$).

with the lattice spacing set to 1. The DOS $\rho_{\square}(\varepsilon)$ which is depicted in Fig. 1(a) can be expressed by a complete elliptic integral of the first kind (see Appendix E). For positive hopping matrix element t the lower band edge is reached at $\underline{k}_{\rm b}=\underline{0}$, while the maxima of the band structure are located at the corners of the square-shaped first Brillouin zone [$\underline{k}_{\rm t}=(\pm\pi,\pm\pi)$]. The logarithmic van Hove singularity at $\varepsilon=0$ corresponds to the saddle points of the dispersion (32). The symmetric shape of the DOS with respect to $\varepsilon=0$ reflects the particle-hole symmetry of the Hubbard model on the square lattice. In the following we make use of this symmetry and consider only the case of a less than half-filled lattice ($0\leqslant n\leqslant 1$) and $t>0$.

Figure 1(b) shows the spin-flip energies at $U=\infty$ resulting from the variational criteria discussed in the previous sections as a function of δ. The Gutzwiller wave function [Eq. (3) with $f=0$] gives a critical hole density $\delta_{\rm cr}=0.4905$ for the instability of the Nagaoka state.[28] For the variational ansatz (3) including nearest-neighbor hopping processes of the majority spins (finite f), the spin-flip energy is considerably lowered and the critical hole density decreases to $\delta_{\rm cr}=0.4155$. The evaluation of the variational state

RES0, which contains *all* spin-up hopping terms of the Basile-Elser type, leads to $\delta_{cr}=0.4045$. Thereby we reproduce up to the fifth digit our result obtained in Ref. 24, where we took into account hopping processes over a distance of up to four lattice spacings.

The fact that the reduction of the spin-flip energy in Fig. 1(b) is mainly due to the nearest-neighbor term demonstrates the overwhelming importance of *local* polarizations of the spin-up Fermi sea for the instability of the Nagaoka state. The resolvent method treats implicitly an *infinite* number of variational parameters and makes it possible to investigate the full Basile-Elser ansatz in the thermodynamic limit. Compared to the iterative method used in Ref. 24 it has the remarkable advantage that the lowest possible spin-flip energy in a given subspace can be calculated *without* explicit knowledge of the corresponding state. As we will see in Sec. III E, it is not generally true that the best value for δ_{cr} within the Basile-Elser subspace can be obtained by restricting the spin-up hopping processes to a small cluster centered at the position of the flipped spin.

Figure 2(a) shows the Nagaoka instability lines in the phase diagram for the Gutzwiller single spin flip (Gw), the nearest-neighbor ansatz (NN) (3) as well as for the wave functions RES1, RES2, and RES3 evaluated by means of the resolvent method. The $\uparrow$-hopping terms appear to be much less efficient in suppressing the Nagaoka state if the hole density is small (because most of the sites near the flipped spin are already occupied by a $\uparrow$ electron) and the on-site repulsion U is finite (because the terms all exclude double occupancies at the down spin position). Since the Gutzwiller projector (with $g>0$) represents the only term contained in RES1 which is relevant for $U<\infty$, the critical on-site repulsion near half filling is only slightly increased and U_{cr} remains finite for $\delta=0$. A remarkable improvement is obtained by allowing for nearest-neighbor exchange processes and thereby taking into account the antiferromagnetic tendency of the nearly half-filled Hubbard model. This is embodied in the ansatz RES2. For a constant nonzero value of the DOS at the upper band edge it leads to the asymptotic behavior $U_{cr,\,red}(\delta)=1-\mathcal{O}(\delta)$ for $\delta\rightarrow 0$. This implies the instability of the Nagaoka state for all finite values of U in this limit. Figure 2(b) shows that the optimum spin-flip energy for RES2 plotted as a function of the hole density for a fixed finite value of U approaches a finite negative value of the order t^2/U at half filling while it vanishes for all wave functions containing only the Gutzwiller projector.

The asymptotic behavior for $\delta\rightarrow 0$ of the spin-flip energy and of the Nagaoka instability line $U_{cr}(\delta)$ is not affected by the extension of the Hilbert subspace to the full resolvent ansatz RES3. As for $U=\infty$ the *local* terms play the most important role in destabilizing Nagaoka ferromagnetism. With increasing hole density exchange processes become less important and the Nagaoka instability lines for RES2 and RES3 approach the one obtained for RES1. Since *all* RES wave functions differ only in the subspace with double occupancies the corresponding instability lines end up with a diverging on-site repulsion U_{cr} at the critical hole density $\delta_{cr}=0.4045$ obtained for RES0.

Figure 2(a) displays also the best known variational bound for the Nagaoka stability regime on the square lattice computed by Wurth *et al.*[23] The corresponding state contains

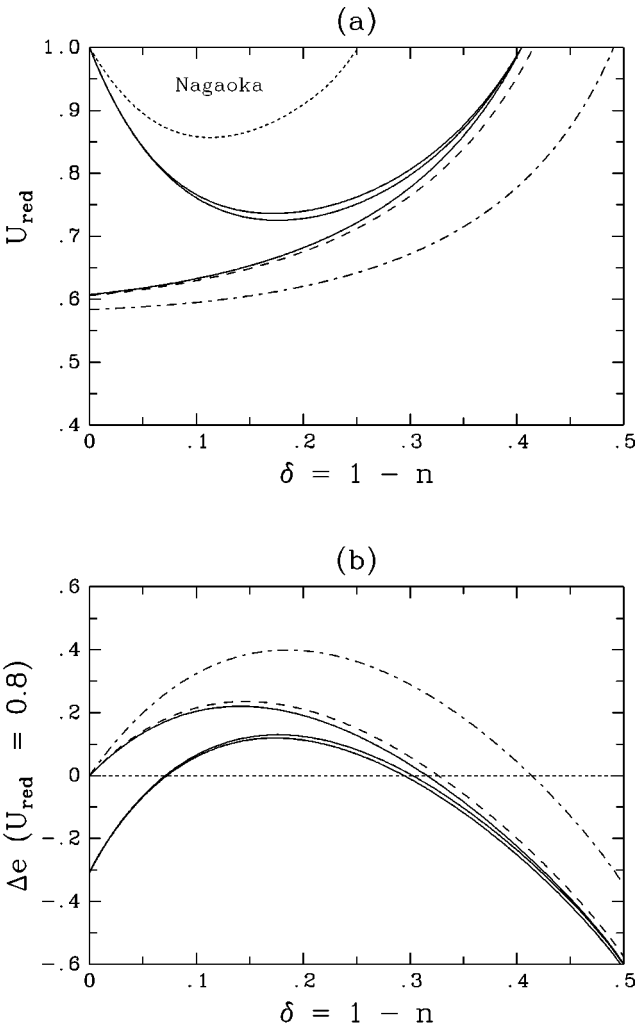

FIG. 2. (a) Phase diagram ($n<1$): Nagaoka instability lines on the square lattice for Gw (dashed-dotted), NN (long-dashed), RES1, RES2, RES3 (full lines, from bottom to top), and the 1100 parameter ansatz of Wurth *et al.* (Ref. 23) (short-dashed), (b) spin-flip energy for $U_{red}=0.8$ and $t=1$ as a function of the hole density for Gw (dashed-dotted), NN (dashed), RES1, RES2, and RES3 (full lines, from top to bottom).

1100 terms, most of them describing excitations of the spin-up Fermi sea with up to two particle-hole pairs located within a 9×9 plaquette around the down-spin position. The critical hole density obtained with this variational wave function is $\delta_{cr}=0.2514$ and the minimum critical on-site repulsion is $U_{cr}^{min}/t=77.74$ (RES3: $U_{cr}^{min}/t=36.21$). Comparing these results one should keep in mind that the resolvent method allows us to derive analytic expressions for the Nagaoka instability line $U_{cr}(\delta)$, at least for RES1 and RES2, while the calculation of the phase boundary for the 1100 parameter state requires an immense numerical effort.

B. Square lattice with next-nearest-neighbor hopping

Extending the Hamiltonian (1) by taking next-nearest-neighbor hopping processes of the electrons into account and introducing a corresponding hopping amplitude $t\beta$ allows us to *create* a particle-hole asymmetry of the DOS. Variation of the ratio $t\beta/t$ makes it possible to simulate a continuous

''transition'' between a bipartite and a nonbipartite lattice. In this subsection we investigate how this transition affects the stability of the Nagaoka state with respect to a Gutzwiller single spin flip on the square lattice. Furthermore we will give a perturbation argument for $|t| \ll |t\prime|$.

The band dispersion of the so-called t-$t\prime$-U model on the square lattice is given by

$$\varepsilon_{t-t\prime}(\underline{k}) = -2t(\cos k_x + \cos k_y) - 4t\prime \cos k_x \cos k_y . \quad (33)$$

For $t,t\prime > 0$ the lower band edge $\varepsilon_b = -4(t+t\prime)$ is reached at $\underline{k}_b = \underline{0}$. The maxima of the band structure are located at the corners of the Brillouin square for $t\prime < t/2$ and at the edge centers for $t\prime > t/2$, respectively. Exactly for $t\prime = t/2$ the maximum single-particle energy $\varepsilon_t = 2t$ is reached at the whole border of the Brillouin zone. This leads to a nesting situation and to the largest possible particle-hole aymmetry with a diverging DOS at the upper band edge. For $t\prime > t/2$ local minima of the band structure develop at the corners of the Brillouin zone leading to a step in the DOS. In the limit $t/t\prime \to 0$ the single-particle energy at these $\underline{k}$ points reaches the lower band edge. The calculation of the DOS $\rho_{t-t\prime}(\varepsilon)$ requires in general a numerical $\underline{k}$ integration. Only for $t\prime = t/2$ is it possible to map $\rho_{t-t\prime}(\varepsilon)$ on the DOS for $t = 0$ and hence on a complete elliptic integral (see Appendix E):

$$\rho_{t-t\prime}(\varepsilon) = \left(1 - \frac{\varepsilon}{2t}\right)^{-1/2} \rho_{\square}\left(2t\sqrt{1 - \frac{\varepsilon}{2t}}\right). \quad (34)$$

The symmetry of the Nagaoka stability regime with respect to half-filling found in the ''pure'' Hubbard model is destroyed if the next-nearest-neighbor hopping $t\prime$ is switched on. In analogy to the nonbipartite triangular and *kagomé* lattices (see Ref. 25 and Sec. III F in this paper) one should expect that the tendency towards saturated ferromagnetism increases for more than half filling and decreases for $n < 1$. The RES ansatzes with the reduction to DOS integrals cannot be used for the t-$t\prime$ model since the $t\prime$ hops go beyond nearest-neighbor hopping.

The calculation of the optimum spin-flip energy for the Gutzwiller ansatz [Eq. (3) with $f = 0$] requires additional effort for the t-$t\prime$-U model due to the more complicated structure of the band dispersion Eq. (33). The kinetic energy of the flipped spin no longer depends only on ε_b but also on the corresponding *momentum* $\underline{k}_b$. For $t,t\prime > 0$ (i.e., for less than half filling) we find $\underline{k}_b = \underline{0}$ as for $t\prime = 0$, whereas for $t,t\prime < 0$ (i.e. for more than half filling) we choose $\underline{k}_b = (\pi,\pi)$ for $t\prime/t \leqslant 1/2$ and $\underline{k}_b = (\pi,0)$ for $t\prime/t > 1/2$.

Figure 3 shows the DOS for the t-$t\prime$-U model on the square lattice and the corresponding Nagaoka instability lines in the phase diagram for various ratios $t\prime/t \leqslant 1/2$. We set $|t| + |t\prime| = 1$ so that the lower band edge is always at $\varepsilon_b = -4$. Increasing $t\prime/t$ leads to a lower DOS at ε_b and a higher DOS at ε_t, while the logarithmic singularity at $\varepsilon = 4t\prime$ approaches the upper band edge. The maximum particle hole asymmetry is reached at $|t\prime/t| = 1/2$ (i.e., $|t\prime| = 1/3$) where the DOS Eq. (34) diverges like $(\sqrt{\varepsilon_t - \varepsilon} \cdot |\ln(\varepsilon_t - \varepsilon)|)^{-1}$ for $\varepsilon \approx \varepsilon_t$. The Nagaoka stability region for less than half filling shrinks as $t\prime/t$ is increased and disappears at $t\prime/t = 1/2$ [Figs. 3(b), 5]. On the other hand, it expands rapidly for $n > 1$, especially in the limit $n = 2$. At

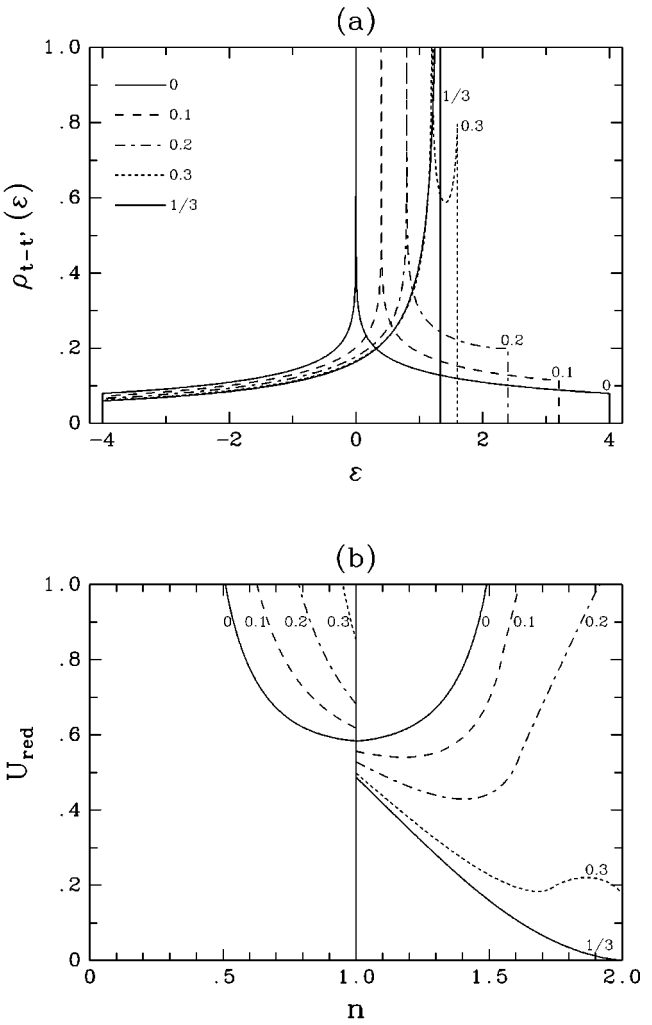

FIG. 3. t-$t\prime$-U model on the square lattice for $|t\prime| \leqslant |t|/2$: $|t\prime| = 1 - |t| = 0, 0.1, 0.2, 0.3, 1/3$: (a) DOS $\rho_{t-t\prime}(\varepsilon)$ for $t,t\prime > 0$ [$\rho_{t-t\prime}(\varepsilon)$ for $t,t\prime < 0$ is obtained by $\varepsilon \leftrightarrow -\varepsilon$], (b) Nagaoka instability lines for a Gutzwiller single spin flip (the curves for $n < 1$ correspond to $t,t\prime > 0$ whereas the curves for $n > 1$ correspond to $t,t\prime < 0$).

$t\prime/t = 1/2$ the Nagaoka state is stable towards a Gutzwiller single spin flip for all $U > 0$ in this limit. Even the slope of the Nagaoka instability line $U_{cr}(n)$ vanishes at $n = 2$.

If one increases the ratio $t\prime/t$ beyond 1/2, the logarithmic singularity in the DOS is gradually shifted back towards $\varepsilon = 0$ and the shape of $\rho_{t-t\prime}(\varepsilon)$ becomes more and more symmetric [Fig. 4(a)]. Nevertheless the step at $\varepsilon = 4t\prime(1 - t/t\prime)$ remains present for all $t/t\prime > 0$. The DOS at $t = 0$ is identical to $\rho_{\square}(\varepsilon)$, which reminds us that the $t\prime$-U model with suppressed nearest-neighbor hopping consists of *two* completely decoupled square lattices.

At $t\prime = t$ the Nagaoka stability region in the phase diagram is found to be still very asymmetric with respect to $n = 1$ [Fig. 4(b)]. A further increase of $t\prime/t$ makes the phase boundaries above and below half filling approach the ones obtained at $t = 0$. Within our variational calculations, the local stability of the saturated ferromagnetic state is identical in both limiting cases $t\prime = 0$ and $t = 0$, but see the perturbative argument below. The step in the DOS, however, leads to a cusp in the Nagaoka stability line $U_{cr}(n)$ for all $|t/t\prime| < 2$. For

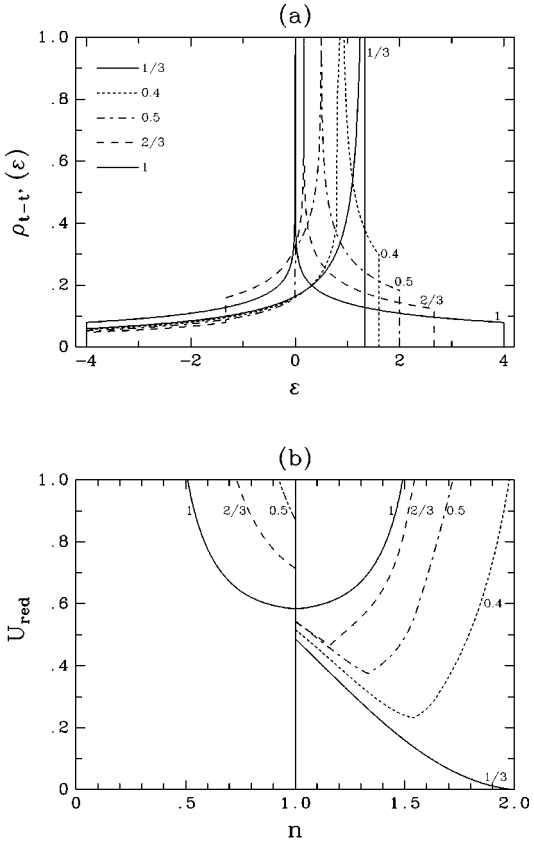

FIG. 4. t-$t\beta$-U model on the square lattice for $|t\beta| \geqslant |t|/2$: $|t\beta| = 1-|t| = 1/3, 0.4, 0.5, 2/3, 1$: (a) DOS $\rho_{t-t\beta}(\varepsilon)$ for $t, t\beta > 0$ [$\rho_{t-t\beta}(\varepsilon)$ for $t, t\beta < 0$ is obtained by $\varepsilon \leftrightarrow -\varepsilon$], (b) Nagaoka instability lines for a Gutzwiller single spin flip (the curves for $n<1$ correspond to $t, t\beta > 0$ whereas the curves for $n>1$ correspond to $t, t\beta < 0$).

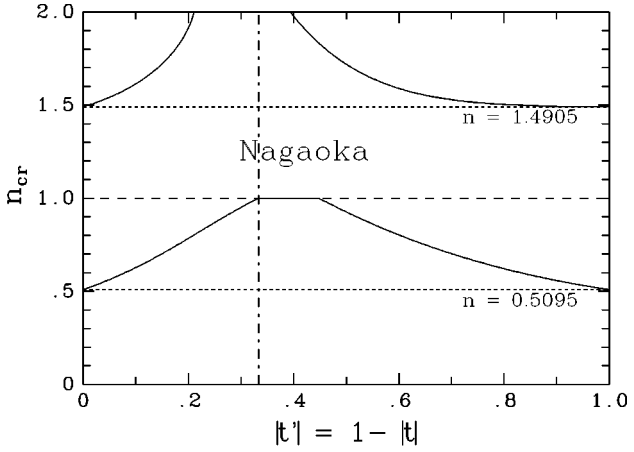

FIG. 5. Critical densities for the Nagaoka instability at $U=\infty$ for a Gutzwiller single spin flip on the square lattice as a function of $|t\beta| = 1-|t|$. Between the two full lines the Nagaoka state is found to be possibly stable. The dashed-dotted line marks the singular case $|t\beta/t| = 1/2$ where the particle-hole asymmetry reaches its maximum.

$t \to 0$, this cusp approaches $n=1$ and $dU_{cr}/dn|_{n=1+}$ is discontinuous at $t=0$. This represents a qualitative difference to the limit $t\beta \to 0$.

In Fig. 5 the upper and lower critical densities for the Nagaoka instability at $U=\infty$ are plotted as functions of $|t\beta| = 1-|t|$. Thereby we once again demonstrate the shift of the Nagaoka stability region towards more than half filling with increasing particle-hole asymmetry in the DOS. The regimes of complete Nagaoka stability for $n>1$ ($-0.21 \leqslant t\beta \leqslant -0.39$) and of complete Nagaoka instability for $n<1$ ($1/3 \leqslant t\beta \leqslant 0.45$) are *not* symmetric with respect to $|t\beta| = 1/3$. There are two different reasons for this asymmetry. First, since the increase of the DOS at the lower band edge is more pronounced for $t\beta \searrow -1/3$ (that is, on the left-hand side of the dashed-dotted line in Fig. 5) than for $t\beta \nearrow -1/3$, also the tendency towards saturated ferromagnetism in the low-density limit (corresponding to $n \to 2$ in Fig. 5) is stronger in the former case. Second, the Nagaoka instability condition near half filling is essentially determined by the ratio $\varepsilon_t/(zt)$, i.e., by the asymmetry of the band edges with respect to $\varepsilon = 0$. The fact that the latter asymmetry is more pronounced for $|t\beta| > 1/3$ than for $|t\beta| < 1/3$ is responsible for the instability of the Nagaoka state for less than half filling on the right-hand side of the dashed-dotted line in Fig. 5.

In the limit $t \to 0$, a perturbative argument gives further insight in the stability of saturated ferromagnetism. Starting point is the observation that at $t=0$ the square lattice decomposes into two independent square lattices tilted by 45° with hopping element $t\beta$. Without any t the two independent Nagaoka states on each sublattice can be oriented arbitrarily without influencing the energy. Thus we deal with a degenerate situation and investigate by $E^{(2)}$ (second-order perturbation coefficient in t) whether the parallel or the antiparallel orientation is favored. The linear order $E^{(1)}$ vanishes for particle-hole symmetry reasons and does not lift the degeneracy.

For the parallel configuration it is straightforward to calculate $E^{(2)}$. Without loss of generality we choose $t\beta = 1/4$ and consider $\varepsilon(k) = \varepsilon_0(k) - 2t[\cos(k_x) \pm \cos(k_y)]$ with $\varepsilon_0(k) = -\cos(k_x)\cos(k_y)$ as dispersion. The plus sign refers to $n<1$, $t\beta > 0$ and the minus sign to $n>1$, $t\beta > 0$. This can be seen by means of a particle-hole transformation and a sign transformation $c_i \to -c_i$ on all sites with an *even* x coordinate. One obtains at constant filling $E^{(2)} = -|\Lambda|/(2t\beta)A_{\pm}(\varepsilon_F)$ with

$$A_{\pm}(\varepsilon_F) = \int_{-\pi}^{\pi} \frac{d^2k}{(2\pi)^2} [\cos(k_x) \pm \cos(k_y)]^2 \times \delta(\varepsilon_F + \cos(k_x)\cos(k_y)) = -\frac{4}{\pi^2}[\pm \varepsilon_F K(1-\varepsilon_F^2) - E(1-\varepsilon_F^2)] \qquad (35)$$

yielding the dotted curves in Fig. 6. The relation (35) is found with the help of the quantities I_n in Appendix A of Hanisch/Müller-Hartmann;[24] K and E are complete elliptic integrals. Note that the coefficient $E^{(2)}$ is not continuous across $n=1$.

Next we assess the energy of two antiparallel Nagaoka states on each of the sublattices. Let us use $a^+_{k,\sigma}$ for the fermions on the A sublattice and $b^+_{k,\sigma}$ for the fermions on the B sublattice. The perturbation reads then

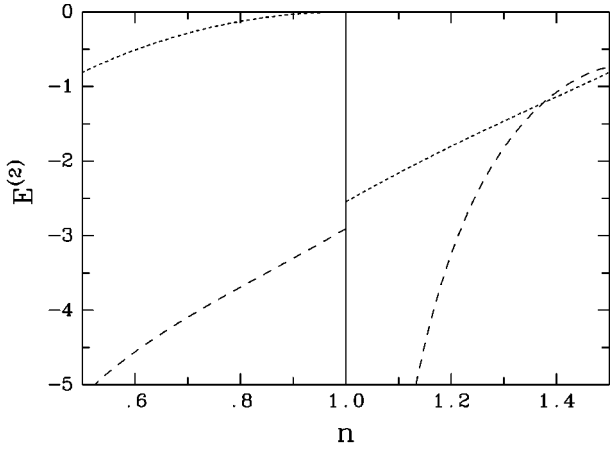

FIG. 6. Second-order perturbation coefficient $E^{(2)}$ in t in units of $4t\delta N$. Dotted line: for parallel Nagaoka states (or global ferromagnetic state, see text); dashed line: upper bound to $E^{(2)}$ for antiparallel Nagaoka states (or global antiferromagnetic state).

$$H_1 = -2t \sum_{\underline{k} \in \mathrm{MBZ}} [\cos(k_x) \pm \cos(k_y)](a^+_{\underline{k},\sigma} b_{\underline{k},\sigma} + b^+_{\underline{k},\sigma} a_{\underline{k},\sigma}), \tag{36}$$

where MBZ is the magnetic Brillouin zone. The second-order energy lowering is

$$E^{(2)} t^2 |\Lambda| = -\langle A\uparrow, B\downarrow | H_1 (H_0 - E_0)^{-1} H_1 | A\uparrow, B\downarrow \rangle. \tag{37}$$

The acronyms $A\uparrow$ and $B\downarrow$ stand for the respective Fermi seas. There are two processes which contribute equally to Eq. (37). Either a fermion is shifted from A to B and back or a fermion is shifted from B to A and back. The latter yields explicitly

$$\begin{aligned} E^{(2)} &= -\frac{8}{|\Lambda|} \sum_{\underline{k} \in \mathrm{MBZ}} [\cos(k_x) \pm \cos(k_y)]^2 \Theta(\varepsilon_F - \varepsilon_0(\underline{k})) \\ &\quad \times \langle A\uparrow | a_{\underline{k},\uparrow} [H_{0,A} - E_{0,A} - \varepsilon(\underline{k})]^{-1} a^+_{\underline{k},\uparrow} | A\uparrow \rangle \\ &= 4 \int \frac{d^2k}{(2\pi)^2} [\cos(k_x) \pm \cos(k_y)]^2 \\ &\quad \times g_{\underline{k}}(\varepsilon_0(\underline{k})) \Theta(\varepsilon_F - \varepsilon_0(\underline{k})), \end{aligned} \tag{38}$$

where $g_{\underline{k}}$ is the one-particle Green function. Now we specify that we work at $U = \infty$ and we *assume* that the Nagaoka state is stable for $t = 0$ at the filling considered. If the Nagaoka state is not stable we do not need to make the present comparison anyway. Based on our assumption, the Green function is purely real and negative. It obeys the inequality

$$g_{\underline{k}}(\varepsilon_0(\underline{k})) < (\varepsilon_0(\underline{k}) - e_{\underline{k}})^{-1} < 0 \tag{39a}$$

$$\begin{aligned} e_{\underline{k}} &:= \langle a_{\underline{k},\uparrow} | H_{0,A} - E_{0,A} | a^+_{\underline{k},\uparrow} \rangle \\ &= -e_1/\delta + \varepsilon_0(\underline{k}) \delta [1 - (e_1/\delta)^2]. \end{aligned} \tag{39b}$$

The estimate (39a) corresponds to a simple Gutzwiller ansatz[28] and yields Eq. (39b) [see Eqs. (4) and (5) with $t = t\delta = 1/4$ and $z = 4$ in Ref. 24]. Thus we obtain

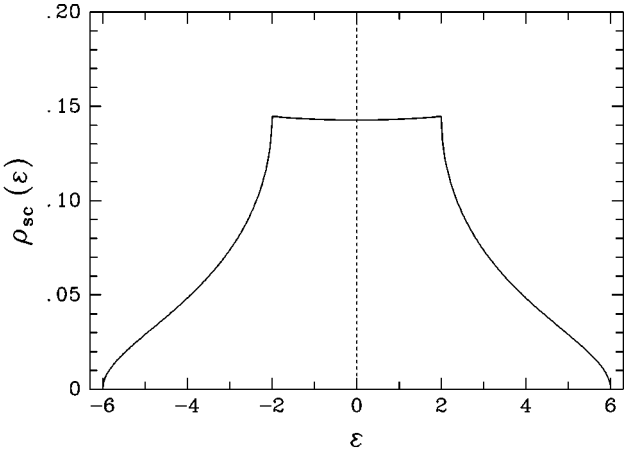

FIG. 7. DOS for the simple cubic lattice ($t = 1$).

$$E^{(2)} < \frac{4\delta}{f} \int_{-1}^{\varepsilon_F} d\varepsilon \frac{A_{\pm}(\varepsilon)}{\lambda - \varepsilon}, \tag{40}$$

where $f = \delta(\delta - 1) - e_1^2$, $\lambda = e_1/f$, and $A_{\pm}$ from Eq. (35). The evaluation of the right-hand side of Eq. (40) yields the dashed curves in Fig. 6. The essence of Fig. 6 is that the saturated ferromagnetic state is unstable in the limit $t \to 0$ for all fillings. The small region where $E^{(2)}_{\mathrm{FM}}$ lies below the upper bound for $E^{(2)}_{\mathrm{AFM}}$ does not count since we know that at these dopings (and for larger dopings) already the pure square lattice at $t = 0$ has no saturated ferromagnetic ground state, see e.g., Refs. 24 and 23.

We wish to draw the reader's attention to the fact that the comparison in Fig. 6 is quite different from the main theme of this paper which is based on single spin-flip energies. Here the global stability is tested with a completely different, antiferromagnetic state. We learn from the perturbative argument that in Fig. 5 the true lines $n(t\delta)$ comprising the *global* Nagaoka stability region have to converge both to the point $t\delta = 1$, $n = 1$.

C. Simple cubic lattice

The energy dispersion of the simple cubic lattice is

$$\varepsilon_{\mathrm{sc}}(\underline{k}) = -2t[\cos(k_x) + \cos(k_y) + \cos(k_z)]. \tag{41}$$

The calculation of $\rho_{\mathrm{sc}}(\varepsilon)$ can be performed by an integration over the known DOS of the square lattice (see Appendix E). The maxima and minima of the energy dispersion (41) are $\varepsilon_{\mathrm{t}} = z|t|$ and $\varepsilon_{\mathrm{b}} = -z|t|$, respectively, with the coordination number $z = 6$. At the band edges the DOS (Fig. 7) shows the square-root behavior which is characteristic for $d = 3$. The van Hove singularities at $\varepsilon = \pm 2t$ correspond to the saddle points of the dispersion (41).

Figure 8(a) shows the spin-flip energy at $U = \infty$ for Gw, NN, and RES0. For small hole doping the loss of spin-up kinetic energy due to the spin flip is sufficiently strong to keep the Nagaoka state stable. With increasing δ the spin-flip energy decreases due to the gain of kinetic energy for the flipped spin which grows linear with δ in leading order. The upper bound for the critical hole density is reduced from $\delta_{\mathrm{cr}} = 0.323$ for Gw (Refs. 28 and 29) to $\delta_{\mathrm{cr}} = 0.247$ for NN and finally to $\delta_{\mathrm{cr}} = 0.237$ for RES0. As in $d = 2$, the NN

hopping term gives the dominant contribution to the decrease of δ_{cr}, while the extension of the spin-up hopping processes to the whole lattice has only a small effect.

Roth[38] investigated the Nagaoka instability with respect to a single spin flip on the sc lattice already in 1969, making use of the so-called two pole approximation instead of the projection method. It was shown later[39,40] that the Hilbert subspace considered in Ref. 38 is equivalent to the Basile-Elser subspace in the limit $U\rightarrow\infty$. Roth obtained numerically a critical hole density of 0.24 which is consistent with our variational result for RES0.

The phase diagram [Fig. 8(b)] for the simple cubic lattice shows a qualitative difference to the square lattice: The critical U at half filling obtained for the Gutzwiller single spin flip is not at all improved by including NN hopping terms. Even for RES1 $U_{cr}(\delta=0)$ is still given by the bandwidth $12|t|$. This is due to the fact that for the sc lattice the DOS at the upper band edge vanishes, while it is nonzero for the square lattice.

As in $d=2$, the ansatz RES2 leads to $U_{cr}(\delta=0)=\infty$ and to a considerable reduction of the Nagaoka stability regime near half filling. For the full resolvent ansatz RES3 we finally achieve a minimum critical coupling of $U_{cr}^{min}=48.9|t|$ (corresponding to $U_{red}=0.753$) below which the Nagaoka state is proven to be unstable for all δ. The region left for a possible Nagaoka ground state on the sc lattice is therefore substantially smaller than on the square lattice (RES3 for the square lattice: $\delta_{cr}=0.405, U_{cr}^{min}=36.2|t|$). Generally the tendency of the Hubbard model towards a saturated ferromagnetic ground state on a d-dimensional hypercubic lattice becomes weaker with increasing d. Müller-Hartmann[30] showed that the critical hole density at $U=\infty$ with respect to a Gutzwiller single spin flip decreases asymptotically as $\delta_{cr}\propto 1/\sqrt{d\ln d}$ for $d\gg 1$. In the limiting case of infinite dimensions the ground state of the Hubbard model is never fully polarized.[41]

D. bcc lattice

The bcc lattice is another interesting example of a three-dimensional bipartite lattice. It has a slightly higher coordination number $z=8$ compared to the simple cubic lattice. Its dispersion reads

$$\varepsilon_{bcc}(\underline{k})=-8t\cos(k_x)\cos(k_y)\cos(k_z). \tag{42}$$

The calculation of the DOS $\rho_{bcc}(\varepsilon)$ can again be performed by an integration over the known DOS of the square lattice (see Appendix E). The bipartiteness is obvious since $\varepsilon_{bcc}(\underline{k}+\underline{Q})+\varepsilon_{bcc}(\underline{k})=0$ with $\underline{Q}=(\pi,\pi,\pi)^{\dagger}$. For this reason we consider only $n\leqslant 1$.

The DOS is shown in Fig. 9(a). The square-root singularities at the band edges are generic for three dimensions. The least common feature for a three-dimensional lattice is the squared logarithmic singularity at zero energy $\rho_{bcc}(\varepsilon)\approx\ln^2(\varepsilon)/(4\pi^3)$ which results from the points in momentum space where all cosines in Eq. (42) vanish, e.g., $\varepsilon_{bcc}(\underline{k})\approx -8t(k_x-\pi/2)(k_y-\pi/2)(k_z-\pi/2)$.

Evaluating Eq. (4) for the bcc lattice, we find the critical density

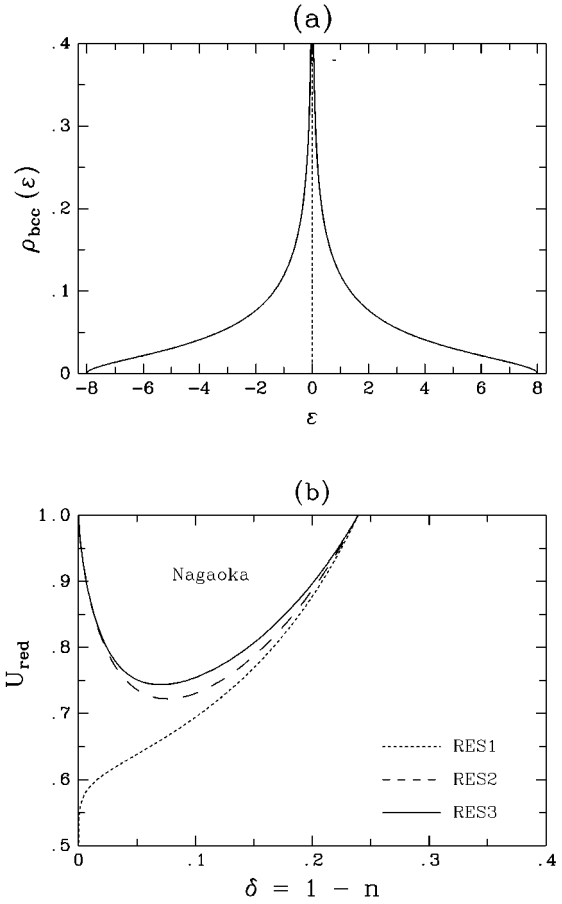

FIG. 9. (a) DOS for the bcc lattice ($t=1$). (b) Phase diagram ($n<1$): Nagaoka instability lines on the bcc lattice for RES1 (dotted line), RES2 (dashed), and RES3 (full line).

E. Honeycomb lattice

Besides the square lattice the honeycomb lattice (see Fig. 9 in Ref. 25) is another prominent example of a bipartite lattice in $d=2$. In contrast to the square lattice it is not a Bravais lattice, however, but a triangular lattice with a two site basis. The coordination number is $z=3$ and the band dispersion reads

$$\varepsilon_{\mathrm{hon}}(\underline{k}) = \pm\sqrt{t[3t-\varepsilon_{\triangle}(\underline{k})]}, \tag{43}$$

where $\varepsilon_{\triangle}(\underline{k})$ stands for the energy dispersion of the triangular lattice to be described in Eq. (44). Despite this additional complication the formulas developed in Sec. II via the resolvent method hold here as well (see Appendix B).

The instability of the Nagaoka state with respect to Gw and NN was already discussed in Ref. 25. Here we present the improvements obtained by the resolvent method. The evaluation of RES0 shows that hopping processes with a larger distance from the down-spin position have only a very small influence on the optimum spin-flip energy at $U=\infty$ (Fig. 10).

The instability gap ($0.379 \leqslant \delta \leqslant 0.481$) between the two possible Nagaoka stability regions remains almost unchanged compared to the result for NN. The upper critical hole density is only slightly improved to $\delta_{\mathrm{cr}}=0.643$ from 0.662 (NN) and 0.802 (Gw).[25]

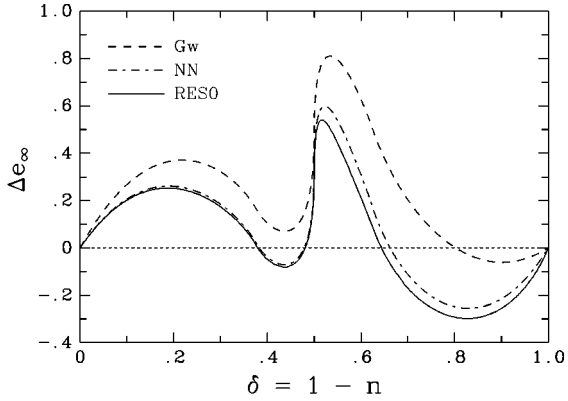

FIG. 10. Spin-flip energy at $U=\infty$ as a function of the hole density on the honeycomb lattice ($t=1$) for Gw, NN, and RES0.

As explained in Ref. 25 the Nagaoka stability island in the phase diagram around quarter filling (Fig. 11) is mainly due to the zero in the DOS at $\varepsilon=0$, i.e., between the two energy bands. Since the lattice structure enters the calculation of the optimum spin-flip energy by means of the resolvent method only via the DOS the stability island is present even for the full resolvent ansatz RES3. On the other hand, the critical U at half filling diverges for RES2 and RES3 and the Nagaoka stability region for small δ shrinks compared to the results for NN and RES1. These results and the pronounced difference between the two minimum values of U ($41.2\,|t|$ for the low doping regime and $17.25\,|t|$ for the stability island) corroborate the previous conjecture[25] that a saturated ferromagnetic ground state exists around quarter filling. The lack of a Nagaoka theorem for the honeycomb lattice[19,25] indicates a degeneracy between the Nagaoka state and other possible states near half filling even at $U=\infty$.

F. Triangular lattice

The triangular lattice is nonbipartite. It can be decomposed into *three* sublattices, each of them having triangular structure. Investigating the local instability of the Nagaoka state towards a Gutzwiller single spin flip a Nagaoka ground state was excluded on the triangular lattice for less than half filling.[29,25] This is in agreement with the Nagaoka theorem, which predicts a saturated ferromagnetic ground state at $U=\infty$ only for the half-filled lattice *plus* an additional electron.

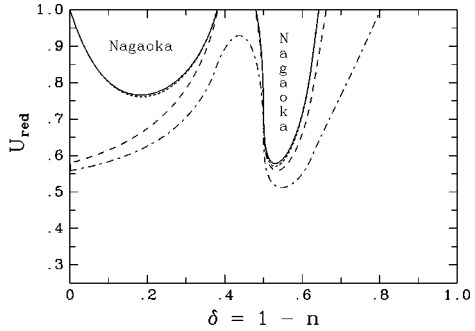

FIG. 11. Phase diagram ($n<1$): Nagaoka instability lines on the honeycomb lattice for Gw (dashed-dotted), NN (long-dashed, almost identical with RES1), RES2 (short-dashed), and RES3 (full line).

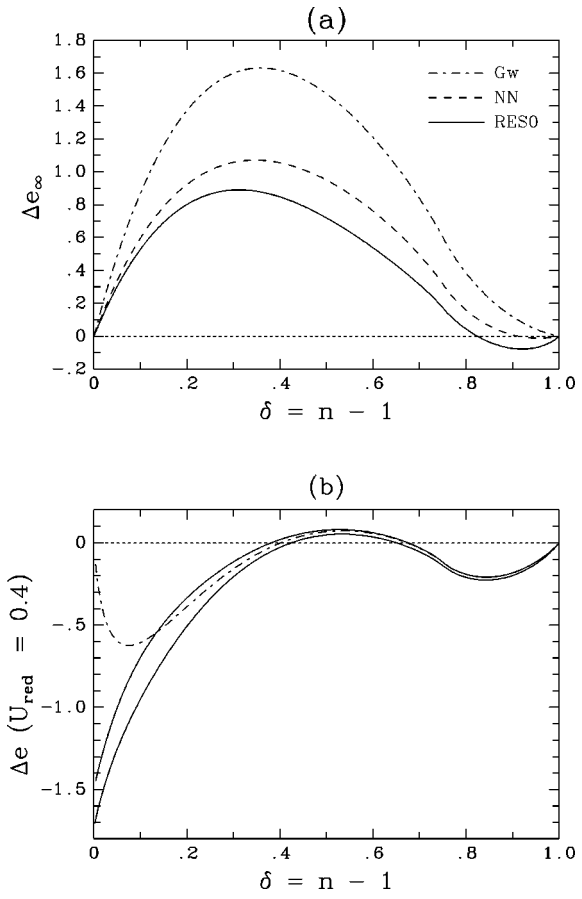

FIG. 12. (a) Spin-flip energy at $U=\infty$ as a function of the hole density on the triangular lattice ($t=-1$) for Gw, NN, and RES0, (b) spin-flip energy at $U_{\mathrm{red}}=0.4$ as a function of the hole density on the triangular lattice ($t=-1$) for RES1 (dashed-dotted line), RES2 (upper full line), and RES3 (lower full line).

Thus we consider henceforth the electron doped case for $t=1$ or, equivalently, $t=-1$ and $n<1$.

Each lattice site has $z=6$ nearest neighbors located at the corners of a hexagon. The band dispersion is given by

$$\varepsilon_{\triangle}(\underline{k}) = 2\cos(k_x) + 4\cos\left(\frac{k_x}{2}\right)\cos\left(\frac{\sqrt{3}k_y}{2}\right), \qquad (44)$$

where $\underline{k}$ belongs to the likewise hexagon-shaped first Brillouin zone. The upper band edge ($\varepsilon_{\mathrm{t}}=6$) is found at the center of the Brillouin zone, whereas the lower band edge $\varepsilon_{\mathrm{b}}=-3$ is reached at the corners of the hexagon. The DOS (see Appendix E and Fig. 1 in Ref. 25), which can be expressed by a complete elliptic integral, displays a logarithmic van Hove singularity at $\varepsilon=-2$. For $\varepsilon_{\mathrm{F}}=-2$ the Fermi surface forms a hexagon with an area of 3/4 of the whole Brillouin zone. As usual in $d=2$ the DOS at the band edges is nonzero [$\rho_{\mathrm{b}}=4\rho_{\mathrm{t}}=(\sqrt{3}\pi)^{-1}$].

In contrast to the square lattice, the Nagaoka state remains stable towards Gw for all fillings $n>1$ at $U=\infty$.[28,29] The corresponding spin-flip energy as a function of δ is depicted in Fig. 12(a). Evaluating NN, however, a negative spin-flip energy is found above $\delta_{\mathrm{cr}}=0.912$ proving the instability of the Nagaoka state in the low-density limit. The resolvent ansatz RES0 lowers the spin-flip energy further and implies

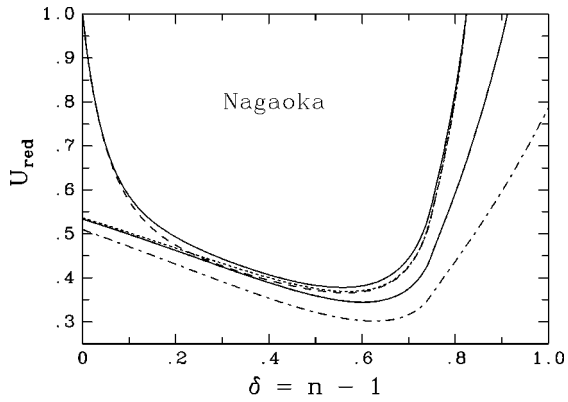

FIG. 13. Phase diagram ($n>1$): Nagaoka instability lines on the triangular lattice for Gw (dashed-dotted), NN (lower full line), RES1 (short-dashed), RES2 (long-dashed), and RES3 (upper full line).

$\delta_{\mathrm{cr}}=0.824$ [Fig. 12(a)]. The difference $\Delta\delta=0.088$ between the results obtained for NN and RES0 is eight times larger than the one for the square lattice ($\Delta\delta=0.011$). This demonstrates the importance of the spin-up hopping processes for the instability of Nagaoka ferromagnetism on the triangular lattice. The reason is that due to the large hole densities under consideration, the probability to find unoccupied sites near the flipped spin is quite high. The same line of reasoning applies also for $U<\infty$, see Fig. 13.

Previously we investigated a variational state which restricts the hopping processes to a 31-site cluster around the position of the flipped spin[25] and obtained $\delta_{\mathrm{cr}}=0.887$. Although the nearest-neighbor processes once again are the most important ones, the number of relevant hopping processes on the triangular lattice turns out to be much larger than on the square lattice. Hence the critical hole density $\delta_{\mathrm{cr}}=0.824$ found by the resolvent method is essentially lower than the one found from the finite cluster calculations. Moreover, the evaluation of RES0 requires much less analytical and numerical effort than the iterative extension of the variational ansatz by additional hopping processes. For details on the application of the resolvent method to the triangular lattice see Appendix C.

Near half filling the influence of the majority spin hopping processes contained in NN and RES1 (which suppress double occupancies) on the Nagaoka stability is negligible, as expected (Fig. 13). In contrast to this the resolvent ansatz RES2 with nearest-neighbor hopping processes *creating* double occupancies leads to a negative spin-flip energy near half filling for all $U<\infty$ and hence to a divergence of $U_{\mathrm{cr}}(n=1)$ (Fig. 13). It turns out, however, that for larger hole densities, when the exchange effect loses its importance, RES2 is somewhat *less* successful than RES1. The plot of the spin-flip energy as a function of δ for the comparatively small on-site repulsion $U_{\mathrm{red}}=0.4$ in Fig. 12(b) demonstrates that above $\delta\simeq 0.12$ the creation of extra holes near the flipped spin as described by RES2 is energetically unfavorable. The full resolvent ansatz RES3, comprising RES1 and RES2, gives of course the best lower bound for the Nagaoka instability line $U_{\mathrm{cr}}(\delta)$. The minimum critical coupling obtained for RES3 is $U_{\mathrm{cr}}^{\mathrm{min}}=9.62|t|$ ($U_{\mathrm{red}}=0.378$), the critical hole density at $U=\infty$ is given by the RES0 value

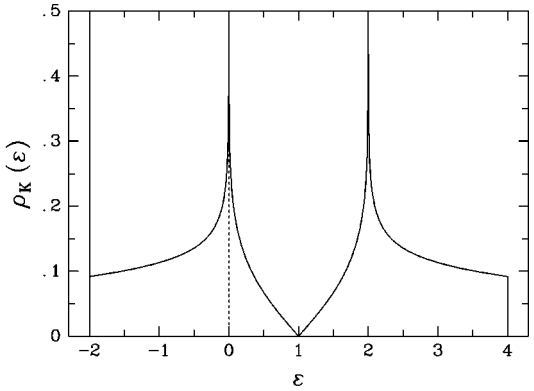

FIG. 14. DOS for the *kagomé* lattice ($t=-1$).

$\delta_{cr}=0.824$. Hence the region for a possible Nagaoka ground state on the triangular lattice appears to be much larger than on the bipartite square and honeycomb lattices.

G. Kagomé lattice

Taking the *kagomé* lattice as an example of a frustrated non-Bravais lattice we want to demonstrate that the resolvent method works also for this class of lattices. Representing the line graph[42] of the honeycomb lattice the *kagomé* lattice (for $t<0$) shows a flat, i.e., dispersionless band with spectral weight 1/3 at the lower band edge $\varepsilon_b=-2|t|$ (Fig. 14). All line graphs display such a flat band.[43] The *kagomé* lattice is the first and the most prominent example of so-called flat-band ferromagnetism.[44,45] A macroscopic degeneracy of the lowest single-particle energy leads for certain band fillings to a unique saturated ferromagnetic ground state. Mielke[43] proved that the Nagaoka state is the unique ground state of the Hubbard model on the *kagomé* lattice for all $U>0$ at $n=1/3$. Although in the flat-band regime every ground state of the Hamiltonian (1) is a simultaneous eigenstate of H_{kin} and H_{pot}, the uniqueness of the ground state is not trivial. For $n<1/3$ the fully polarized ground state is not unique.[4]

The *kagomé* lattice can be considered as a triangular lattice with a basis of three lattice points,[25] see also Appendix D. Besides the flat band $\varepsilon(\underline{k})=2t$ the diagonalization of H_{kin} leads to the two dispersive bands

$$\varepsilon_K(\underline{k})=-t[1\pm\sqrt{3-\varepsilon_\triangle(\underline{k})/t}], \tag{45}$$

where $\varepsilon_\triangle(\underline{k})$ stands for the dispersion (44) of the triangular lattice. For the *kagomé* lattice the resolvent method requires less effort than for the triangular lattice with $t<0$ since the lower band edge $\varepsilon_b=-2|t|$ is reached at $\underline{k}_b=\underline{0}$ for one dispersive band and for the flat band of course. Thus $\underline{q}=\underline{0}$ is the optimum momentum as for bipartite lattices. Hence all lattice-dependent quantities appearing in our formulas can be calculated as integrals over the DOS $\rho_K(\varepsilon)$. For $t=-1$ one finds the DOS of the *kagomé* lattice (see Fig. 14 and Appendix E) as

$$\rho_K(\varepsilon)=\frac{1}{3}\delta(\varepsilon+2)+\frac{2}{3}|\varepsilon-1|\cdot\rho_\triangle[(\varepsilon-1)^2-3]; \tag{46}$$

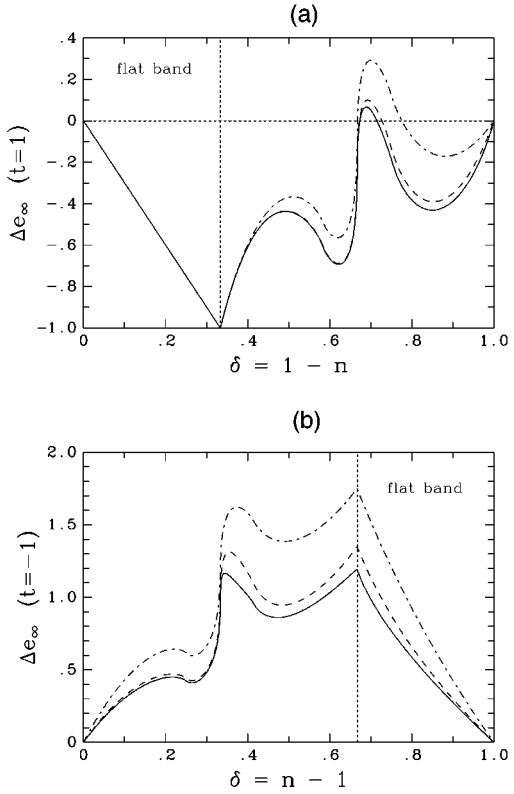

FIG. 15. Spin-flip energy at $U=\infty$ as a function of the hole density on the *kagomé* lattice for Gw (dashed-dotted), NN (dashed), and RES0 (a) for $t=1$, (b) for $t=-1$.

$\rho_\triangle(\varepsilon)$ is the DOS of the triangular lattice. Nevertheless, the fact that the *kagomé* lattice is *not* a Bravais lattice induces some changes in the analytic expressions for the spin-flip energy (Appendix D).

Figure 15(b) shows the spin-flip energy for $U=\infty$ and $t=-1$ as a function of δ for RES0 compared to the Gw and NN results obtained in Ref. 25. As for the honeycomb lattice the enhancement of the Nagaoka stability for $\delta\to 1/3$ is due to the zero in the DOS. The effect of the additional spin-up hopping processes contained in RES0 is most pronounced for $\delta>1/3$. But the spin-flip energy remains positive for all band fillings. Note that the exact result in the flat-band regime is a zero spin-flip energy.[4,25] The phase diagram for $n>1$ in Fig. 16 shows a strong tendency towards Nagaoka ferromagnetism also beyond the flat-band regime, where we find the Nagaoka state to be stable for all $U>0$. There is only a marginal difference between the Nagaoka instability lines for NN and for RES1, since the values of U under consideration are too small to allow a significant reduction of the spin-flip energy by Basile-Elser hopping processes. Near half filling, however, we are able to restrict the Nagaoka stability region by RES2, i.e., by taking antiferromagnetic exchange processes into account. As for the triangular lattice, for a certain range of filling around $n=3/2$ away from half filling RES2 gives a weaker bound for $U_{cr}(\delta)$ than RES1.

For positive hopping matrix element t the flat band is found at the *upper* band edge. The flat-band regime for $n<1$ corresponds to hole densities $0\leqslant\delta\leqslant 1/3$. Since $\underline{k}_b=\underline{0}$ *and* $\varepsilon_b=-zt$ the resolvent method formulas are those of the bipartite lattices (see Appendix B). Figures 15(a) and 16

show that the small Nagaoka stability island found previously[25] for very large U around quarter filling is still

Also for low and intermediate hole doping the extension of the Gutzwiller wave function by nearest-neighbor hopping processes yields only a slight reduction of the Nagaoka stability region in the phase diagram. This is in sharp contrast, for example, to the situation on the sc lattice. The resolvent method was not applied to the fcc and hcp lattices since three-dimensional momentum integrals would have to be performed in order to calculate $h(\omega)$ and $\overline{h}(\omega)$ (see Appendix C).

As for the square lattice (see Sec. III B) the particle-hole asymmetry of the DOS is even enhanced if one extends H_{kin} by electron hopping between *next-nearest-neighbor sites* with a hopping amplitude t'. On the fcc lattice, these sites form a simple cubic structure such that the additional contribution to the dispersion exactly compensates the second term on the right-hand side of Eq. (48) if $t'=t/2$. In this case the DOS for the t-t'

even

depending only on ω and ε_F, but not on the indices $\underline{k}_1$ and $\underline{k}_2$. We define the vector $\underline{w}$ by $(\underline{w})_{\underline{k}} := |\Lambda|^{-1/2}\varepsilon(\underline{k})/(zt)$ for $\underline{k} \in$ FS. Making use of this definition, Eqs. (31), (A2), and (A6) the matrix $\mathbf{B_2}^{-1}$ reads

$$\mathbf{B_2}^{-1} = \mathbf{d_2}^{-1} + (\omega + zt - U)\underline{u}\underline{u}^+ - \alpha(\underline{u}\underline{u}^+ - \underline{u}\underline{w}^+ - \underline{w}\underline{u}^+ + \underline{w}\underline{w}^+). \tag{A8}$$

The off-diagonal elements of $\mathbf{B_2}^{-1}$ do not depend explicitly on $\underline{k}_1$ and $\underline{k}_2$. In contrast to RES0 (12), however, they are not overall constant but take specific values for each block of $\mathbf{B_2}^{-1}$. To overcome this additional complication we introduce the 2×2 matrix

$$\mathbf{A} = \begin{bmatrix} a_1 & a_3 \\ a_3 & a_2 \end{bmatrix} = \begin{bmatrix} \alpha - \omega - zt - U & -\alpha \\ -\alpha & \alpha \end{bmatrix} \tag{A9}$$

and write $\mathbf{B_2}^{-1}$ as $\mathbf{B_2}^{-1} = \mathbf{d_2}^{-1} - \underline{y}^+\mathbf{A}\underline{y}$ with $\underline{y}^+ := (\underline{u}, \underline{w})$. In order to obtain $\mathbf{B_2}$ we use an expansion trick similar to Eq. (14b):

$$\begin{aligned} \mathbf{B_2} &= \mathbf{d_2}(\mathbf{1} - \underline{y}^+\mathbf{A}\underline{y}\mathbf{d_2})^{-1} \\ &= \mathbf{d_2}(\mathbf{1} - \underline{y}^+\mathbf{A}\underline{y}\mathbf{d_2} + \underline{y}^+\mathbf{A}\underline{y}\mathbf{d_2}\underline{y}^+\mathbf{A}\underline{y}\mathbf{d_2} + \cdots) \\ &= \mathbf{d_2} + \mathbf{d_2}\underline{y}^+\mathbf{A}(\mathbf{1} - \mathbf{B}\mathbf{A})^{-1}\underline{y}\mathbf{d_2}, \end{aligned} \tag{A10}$$

with $\mathbf{B} := \underline{y}\mathbf{d_2}\underline{y}^+$ representing the 2×2 matrix

$$\mathbf{B} = \begin{bmatrix} b_1 & b_3 \\ b_3 & b_2 \end{bmatrix} = \begin{bmatrix} \underline{u}^+\mathbf{d_2}\underline{u} & \underline{u}^+\mathbf{d_2}\underline{w} \\ \underline{u}^+\mathbf{d_2}\underline{w} & \underline{w}^+\mathbf{d_2}\underline{w} \end{bmatrix}. \tag{A11}$$

While inverting the matrix

$$\mathbf{1} - \mathbf{B}\mathbf{A} = \begin{bmatrix} c_1 & c_3 \\ c_4 & c_2 \end{bmatrix} = \begin{bmatrix} 1 - a_1b_1 - a_3b_3 & -a_3b_1 - a_2b_3 \\ -a_1b_3 - a_3b_2 & 1 - a_2b_2 - a_3b_3 \end{bmatrix} \tag{A12}$$

represents a simple algebraic task, the elements of $\mathbf{B}$ have to be computed by numerical integration. In analogy to $h(\omega) = \underline{v}^+\mathbf{d_1}\underline{v}$ [see Eq. (16a)] we introduce

$$\overline{h(\omega)} := \underline{u}^+\mathbf{d_2}\underline{u} = |\Lambda|^{-1}\sum_{\underline{k}\in \mathrm{FS}} [\delta(\omega - U) + \overline{\gamma\varepsilon}(\underline{k}) + e_1]^{-1} \tag{A13}$$

with $\overline{\gamma} := \delta - e_1/(zt)$. Just as $h(\omega)$, $\overline{h(\omega)}$ reduces to an integral over the DOS:

$$\overline{h(\omega)} = \int_{\varepsilon_b}^{\varepsilon_F} \frac{\rho(\varepsilon)d\varepsilon}{\delta(\omega - U) + e_1 + \overline{\gamma\varepsilon}} = \overline{\gamma}^{-1}\overline{G(\Omega)}, \tag{A14}$$

with

$$\overline{G(y)} := \int_{\varepsilon_b}^{\varepsilon_F} \frac{\rho(\varepsilon)d\varepsilon}{y + \varepsilon}, \quad \overline{\Omega} := \frac{\delta(\omega - U) + e_1}{\overline{\gamma}}. \tag{A15}$$

The symmetry of the DOS with respect to $\varepsilon = 0$ allows us to map $\overline{G(y)}$ to the integral $G(y)$ already defined in Eq. (16d). Following Eq. (A11), the elements of the matrix $\mathbf{B}$ are given by $b_1 = \overline{\gamma}^{-1}\overline{G(\Omega)}$, $b_2 = \overline{\gamma}^{-1}(zt)^{-2}[e_1 - n\overline{\Omega} + \overline{\Omega^2 G(\Omega)}]$, and $b_3 = (\overline{\gamma}zt)^{-1}[n - \overline{\Omega G(\Omega)}]$.

To find the energy of the bound state we have to solve the equation $(\underline{u}^+\mathbf{B_2}\underline{u})^{-1} \doteq 0$. Starting from Eq. (A10) and writing $\underline{u}$ formally as $\underline{u} = \underline{y}^+\underline{e}_1$ we obtain

$$\begin{aligned} \underline{u}^+\mathbf{B_2}\underline{u} &= \underline{e}_1^+\underline{y}[\mathbf{d_2} + \mathbf{d_2}\underline{y}\mathbf{A}(\mathbf{1} - \mathbf{B}\mathbf{A})^{-1}\underline{y}\mathbf{d_2}]\underline{y}^+\underline{e}_1 \\ &= \underline{e}_1^+[\mathbf{1} + \mathbf{B}\mathbf{A}(\mathbf{1} - \mathbf{B}\mathbf{A})^{-1}]\mathbf{B}\underline{e}_1 \\ &= \underline{e}_1^+(\mathbf{1} - \mathbf{B}\mathbf{A})^{-1}\mathbf{B}\underline{e}_1 \end{aligned} \tag{A16}$$

and, using Eq. (A12), we finally obtain the equation

$$c_4c_3 - c_1c_2 \doteq 0 \tag{A17}$$

for the lower edge of the spectrum of $g_{\underline{k}_b}(\omega)$. After inserting all terms Eq. (A17) takes the form

$$p_1 \cdot \overline{G(\Omega)} - p_2 \doteq 0 \tag{A18}$$

with

$$p_1 = \alpha\overline{\gamma}(\overline{\Omega} + zt)^2 - (\omega + zt - U)[\overline{\gamma}(zt)^2 - \alpha(e_1 + n\overline{\Omega})]$$

$$p_2 = \alpha\overline{\gamma}[n(\overline{\Omega} + 2xt + e_1) + n^2(\omega + zt - U)] + \overline{\gamma^2}(zt)^2.$$

Making use of the identities $\omega + zt - U = \overline{\gamma}\overline{\delta}^{-1}(\overline{\Omega} + zt)$, $e_1 = zt(n - \gamma)$ and introducing $\chi := \alpha\gamma + zt\overline{\gamma}$, Eq. (A18) simplifies to

$$\frac{1}{\delta + (\overline{\Omega} + zt)\overline{G(\Omega)}} \doteq 1 - \frac{zt\chi}{\alpha(\overline{\Omega} + zt)}. \tag{A19}$$

From the definition of α Eq. (A7) we derive the expression

$$\chi = (\Omega + zt)\left(1 - \frac{1}{n + (\Omega + zt)G(\Omega)}\right) \tag{A20}$$

for χ. We *define* in analogy

$$\overline{\chi} := (\overline{\Omega} + zt)\left(1 - \frac{1}{\delta + (\overline{\Omega} + zt)\overline{G(\Omega)}}\right) \tag{A21}$$

and write Eq. (A19) as $\overline{\chi} \doteq zt\chi/\alpha$. The eliminination of α finally leads to the simple result

$$\frac{1}{zt} \doteq \frac{\gamma}{\chi} + \frac{\overline{\gamma}}{\overline{\chi}}. \tag{A22}$$

The Nagaoka instability line $U_{cr}(\delta)$ is obtained by assuming $\omega = \varepsilon_F$ for a given Fermi energy, calculating γ, $\overline{\gamma}$, and χ and solve Eq. (A22) numerically with respect to $\overline{\chi}$. Note that U enters Eq. (A22) solely via $\overline{\Omega}$ and hence via $\overline{\chi}$. To compute the *optimum spin-flip energy* for RES3 for fixed values U and δ, we solve Eq. (A22) with respect to ω and subtract the Fermi energy ε_F from the solution $\omega_0(U, \delta)$.

APPENDIX B: GENERAL UNFRUSTRATED LATTICE

In this appendix it will be shown that the formulas derived in Sec. II and the formulas (A20)–(A22) apply to all unfrustrated, isotropic, homogeneous lattices with nearest-neighbor hopping. In this context, ''homogeneous'' means that all sites are equivalent; ''isotropic'' means that all bonds in all

directions are equivalent. ''Unfrustrated'' means that the state $c_0:=|\Lambda|^{-1/2}\Sigma_{\underline{i}}a_{\underline{i}}$ is an eigenstate of the kinetic Hamiltonian with eigenenergy $\varepsilon_b=-z|t|$ where t is the hopping element as in Eq. (1) and z is the coordination number. This requires $t>0$, hence the absence of frustration. Note that the lattice does not need to be a Bravais lattice. The Bethe lattice, however, is not unfrustrated for $z>1$ in the above sense since its lower band edge is $\varepsilon_b=-2\sqrt{z-1}|t|$,[48] and not $\varepsilon_b=-z|t|$.

Let us denote by c_α^+ the creation operators which diagonalize the kinetic energy

$$\varepsilon_\alpha c_\alpha^+=[H_{\rm kin},c_\alpha^+] \tag{B1}$$

and by $a_{\underline{j}}^+$ the site-diagonal creation operators. The unitary transformation between these two bases has the matrix elements $f_{\alpha,\underline{j}}$

$$c_\alpha^+=\sum_{\underline{j}} f_{\alpha,\underline{j}}a_{\underline{j}}^+, \tag{B2}$$

which implies the expectation values with respect to the Nagaoka state $|\mathcal{N}\rangle$

$$\langle c_{\alpha\uparrow}a_{\underline{j}\uparrow}^+\rangle=f_{\alpha;\underline{j}}^+ \quad \text{for } \varepsilon_\alpha>\varepsilon_F, \tag{B3a}$$

$$\langle a_{\underline{j}\uparrow}^+c_{\beta\uparrow}\rangle=f_{\beta;\underline{j}}^+ \quad \text{for } \varepsilon_\beta<\varepsilon_F. \tag{B3b}$$

The homogeneity required implies that

$$\sum_\alpha |f_{\alpha,\underline{j}}|^2\delta(\omega-\varepsilon_\alpha)=\text{const} \tag{B4}$$

on the lattice, i.e., it does not depend on $\underline{j}$. Unitarity yields furthermore

$$\sum_\alpha |f_{\alpha,\underline{j}}|^2=1. \tag{B5}$$

First we address RES0 with the ansatz ($\varepsilon_\alpha>\varepsilon_F$)

$$\Phi_\alpha:=\sum_{\underline{j}} a_{\underline{j}\uparrow}c_{\alpha\uparrow}^+a_{\underline{j}\downarrow}^+|\mathcal{N}\rangle f_{\alpha,\underline{j}}^+. \tag{B6}$$

The resulting matrix elements are obtained by Wick's theorem and re-expressed with the help of Eqs. (B3a)–(B5)

$$\mathbf{P}_{\alpha\beta,\alpha}=n\delta_{\alpha\beta,\alpha}+\sum_{\underline{j}} |f_{\alpha\beta,\underline{j}}|^2|f_{\alpha,\underline{j}}|^2, \tag{B7a}$$

$$\mathbf{L}_{\uparrow\alpha\beta,\alpha}=(n\varepsilon_\alpha-e_1)\delta_{\alpha\beta,\alpha}, \tag{B7b}$$

$$\mathbf{L}_{\downarrow\alpha\beta,\alpha}=-\frac{e_1\varepsilon_\alpha}{zt}\delta_{\alpha\beta,\alpha}-t\sum_{\langle\underline{i},\underline{j}\rangle} |f_{\alpha\beta,\underline{i}}|^2|f_{\alpha,\underline{j}}|^2. \tag{B7c}$$

The matrix inversion to be solved is

$$(\omega\mathbf{P}-\mathbf{L})^{-1}=(\mathbf{D}^{-1}+\mathbf{N})^{-1}, \tag{B8a}$$

$$\mathbf{D}_{\alpha\beta,\alpha}=\delta_{\alpha\beta,\alpha}[n(\omega-\varepsilon_\alpha)+e_1+(e_1/zt)\varepsilon_\alpha]^{-1}, \tag{B8b}$$

$$\mathbf{N}_{\alpha\beta,\alpha}=\omega\sum_{\underline{j}} |f_{\alpha\beta,\underline{j}}|^2|f_{\alpha,\underline{j}}|^2+t\sum_{\langle\underline{i},\underline{j}\rangle} |f_{\alpha\beta,\underline{i}}|^2|f_{\alpha,\underline{j}}|^2. \tag{B8c}$$

It can be re-expressed with the help of the matrices $\mathbf{M}$, $\mathbf{A}$, and $\mathbf{V}$

$$\mathbf{M}_{\underline{i},\underline{j}}:=\sum_\alpha \frac{|f_{\alpha,\underline{i}}|^2|f_{\alpha,\underline{j}}|^2}{n(\omega-\varepsilon_\alpha)+e_1+(e_1/zt)\varepsilon_\alpha}, \tag{B9a}$$

$$\mathbf{A}_{\underline{i},\underline{j}}:=\omega\delta_{\underline{i},\underline{j}}+t\sum_{\underline{\delta}} \delta_{\underline{i}+\underline{\delta},\underline{j}}, \tag{B9b}$$

$$\mathbf{V}_{\alpha,\underline{j}}:=|f_{\alpha,\underline{j}}|^2, \tag{B9c}$$

where the $\underline{\delta}$ are all spatial vectors connecting nearest neighbors. One obtains

$$(\omega\mathbf{P}-\mathbf{L})^{-1}=\mathbf{D}-\mathbf{DVA}\left(\sum_{n=0}^{\infty}(-\mathbf{MA})^n\right)\mathbf{V}^+\mathbf{D}. \tag{B10}$$

The key observation at this stage is that the vector u with $u_{\underline{j}}=|\Lambda|^{-1/2}$ is an eigenvector both of the matrices $\mathbf{M}$ and $\mathbf{A}$. The corresponding eigenvalue for $\mathbf{M}$ is found with the help of Eq. (B4)

$$h(\omega)=\frac{1}{L}\sum_{\alpha,\underline{i},\underline{j}}\frac{|f_{\alpha,\underline{i}}|^2|f_{\alpha,\underline{j}}|^2}{n(\omega-\varepsilon_\alpha)+e_1+(e_1/zt)\varepsilon_\alpha}, \tag{B11}$$

which simplifies due to Eq. (B5) in the end to the form (16a). The corresponding eigenvalue of $\mathbf{A}$ is $\omega+zt=\omega-\varepsilon_b$. So the series in Eq. (B10) yields a vanishing denominator for $0=1+(\omega-\varepsilon_b)h(\omega)$. Thus we derived Eq. (15) for a much broader class of lattices.

The equations for RES1 and RES2 follow in analogy to the derivation in Sec. II B. The ansatz RES1 is identical to Eq. (18) for $\underline{k}_b=\underline{0}$ and the additional matrix elements are the same as in Eq. (20) once $\varepsilon_{\underline{k}}$ is replaced by ε_α. An important point to note is that the homogeneity (B4) ensures that N_α couples indeed to the constant eigenvector $\underline{u}$

$$(\mathbf{V}^+\mathbf{DN})_{\underline{j}}=[\delta-h(\omega)n(\omega-\varepsilon_b)]u_{\underline{j}} \tag{B12}$$

for which the series summation in Eq. (B10) was achieved.

For the ansatz RES2 we work with Eq. (25) for $\underline{k}_b=\underline{0}$ and find the matrix elements (26) after replacing $\varepsilon_{\underline{k}}$ by ε_α. Using

$$(\mathbf{V}^+\mathbf{DN})_{\underline{j}}=yu_{\underline{j}} \tag{B13}$$

with y as in Eq. (27c), we obtain again Eq. (28) as condition for the variational spin-flip energy.

Let us now turn to RES3. We use ($\varepsilon_\beta<\varepsilon_F$)

$$\Psi_\beta=\sum_{\underline{j}} a_{\underline{j}\uparrow}^+c_{\beta\uparrow}a_{\underline{j}\downarrow}^+|\mathcal{N}\rangle f_{\beta,\underline{j}} \tag{B14}$$

in analogy to Eq. (29) for the doubly occupied states. The matrices $\mathbf{D_1}$ for Φ_α and $\mathbf{D_2}$ for Ψ_β as in Eq. (30) are given by

$$(\mathbf{D_1})_{\alpha\underline{\beta},\alpha} = \delta_{\alpha\underline{\beta},\alpha}[n(\omega-\varepsilon_\alpha)+e_1+e_1\varepsilon_\alpha/(zt)]$$

$$+\omega\sum_{\underline{j}}|f_{\alpha\underline{\beta},\underline{j}}|^2|f_{\alpha,\underline{j}}|^2+t\sum_{\langle\underline{j},\underline{j}\rangle}|f_{\alpha\underline{\beta},\underline{i}}|^2|f_{\alpha,\underline{j}}|^2, \tag{B15a}$$

$$(\mathbf{D_2})_{\beta\underline{\beta},\beta} = \delta_{\beta\underline{\beta},\beta}[\delta(\omega-U+\varepsilon_\beta)+e_1-e_1\varepsilon_\beta/(zt)]$$

$$+\omega\sum_{\underline{j}}|f_{\beta\underline{\beta},\underline{j}}|^2|f_{\beta,\underline{j}}|^2+t\sum_{\langle\underline{j}}$$

$$c_1 := \underline{a}^+ \mathbf{C_1} \underline{a} = \frac{zt}{1+(\omega-\varepsilon_b)h_0} \times \left(h_0 + \frac{2h_1}{zt} + \frac{1}{zt}[h_2 + (\omega-\varepsilon_b)(h_2 h_0 - h_1^2)] \right), \tag{B27a}$$

$$c_2 := \underline{b}^+ \mathbf{C_2} \underline{b} = \frac{zt}{1+(\omega-U-\varepsilon_b)\overline{h_0}} \times \left(\overline{h_0} - \frac{2\overline{h_1}}{zt} + \frac{1}{zt}[\overline{h_2} + (\omega-U-\varepsilon_b)(\overline{h_2}\,\overline{h_0} - \overline{h_1^2})] \right). \tag{B27b}$$

The condition for the singularity of Eq. (B18) reads now

$$1 \doteq c_1 c_2, \tag{B28}$$

which is equivalent to Eq. (A22) as can be shown by some tedious, but straightforward calculation. Thus we have completed the proof that the equations for RES0–3 derived in the main text for hypercubic lattices hold for all unfrustrated, isotropic, homogeneous lattices with nearest-neighbor hopping. Only the coordination number and the DOS enter the evaluation of the RES ansatzes.

APPENDIX C: TRIANGULAR LATTICE

For the triangular lattice with $t<0$ the lower band edge $\varepsilon_b = -3|t|$ is reached at $\underline{k}_b = (4\pi/3, 0)$. Since $\underline{k}_b \neq \underline{0}$, the integral

$$h(\omega) = \left\langle \frac{1}{n[\omega-\varepsilon(\underline{k})] + e_1[1-\varepsilon(\underline{k}-\underline{k}_b)/(zt)]} \right\rangle_{\underline{k}\in \mathrm{BZ}\setminus\mathrm{FS}} \tag{C1}$$

cannot be mapped onto a one-dimensional integral over the DOS but has to be evaluated explicitly in momentum space.

The optimum spin-flip energy for RES0 for a given hole density δ follows from the solution ω_0 of the equation $1+(\omega-\varepsilon_b)h(\omega) \doteq 0$ as $\Delta e_\infty(\delta) = \omega_0 - \varepsilon_F$ (see Sec. II). To obtain the Fermi energy corresponding to the critical hole density δ_{cr} the equation $1+(\varepsilon_F-\varepsilon_b)h(\varepsilon_F) \doteq 0$ has to be solved numerically.

For RES1, Eq. (23) holds also for $\underline{k}_b \neq \underline{0}$, since $|\Lambda|^{-1}\Sigma_{\underline{k}} \varepsilon(\underline{k}-\underline{k}_b) = \varepsilon_b e_1/(zt)$ due to the symmetry of the lattice. Calculating $\underline{N}^+ \mathbf{D_1}^{-1} \underline{N}$ for RES2, however, the integrals

$$h_n = \left\langle \frac{\varepsilon^n(\underline{k})}{n[\omega-\varepsilon(\underline{k})] + e_1[1-\varepsilon(\underline{k}-\underline{k}_b)/(zt)]} \right\rangle_{\underline{k}\in \mathrm{BZ}\setminus\mathrm{FS}}, \tag{C2}$$

which for $\underline{k}_b = \underline{0}$ simplify to Eq. (B22) have to be computed for $n=1,2$. Although the outline of the derivation remains unchanged, this causes some differences in the analytic expressions for the optimum spin-flip energy and the Nagaoka instability line compared with the case $\underline{k}_b = \underline{0}$ (see Sec. II).

Evaluating the full resolvent ansatz RES3, the product in the second line of Eq. (A4) can be written as

$$\varepsilon_b^2 \left[1 + \frac{\varepsilon(\underline{k}_1)}{\varepsilon_b} - \frac{\varepsilon(\underline{q}_1)}{\varepsilon_b}\left(1 + \frac{\varepsilon(\underline{k}_1)}{4\varepsilon_b}\right) \right] \times \left[1 + \frac{\varepsilon(\underline{k}_2)}{\varepsilon_b} - \frac{\varepsilon(\underline{q}_2)}{\varepsilon_b}\left(1 + \frac{\varepsilon(\underline{k}_2)}{4\varepsilon_b}\right) \right], \tag{C3}$$

making use of $\varepsilon_b = -z|t|/2$. The permutation symmetry with respect to the primitive lattice vectors which is essential for the factorization $\varepsilon(\underline{k}-\underline{q}) = -\varepsilon(\underline{k})\varepsilon(\underline{q})/(zt)$ holds also for the triangular lattice. The matrix $\mathbf{N}^+ \mathbf{D_1}^{-1} \mathbf{N}$ is calculated to be

$$\mathbf{N}^+ \mathbf{D_1}^{-1} \mathbf{N} = \alpha_1 \underline{\underline{u}}\,\underline{\underline{u}}^+ + \alpha_2 (\underline{\underline{u}}\,\underline{\underline{w}}^+ + \underline{\underline{w}}\,\underline{\underline{u}}^+) + \alpha_2 \underline{\underline{w}}\,\underline{\underline{w}}^+ \tag{C4}$$

with

$$\alpha_1 = \varepsilon_b^2 - 2\varepsilon_b h_1 + h_2 = H[\varepsilon_b h - h_1]^2, \tag{C5a}$$

$$\alpha_2 = \varepsilon_b^2 h - \frac{5}{4}\varepsilon_b h_1 + \frac{1}{4}h_2 - H\left[\varepsilon_b^2 h^2 - \frac{5}{4}\varepsilon_b h h_1 + \frac{1}{4}h_1^2\right], \tag{C5b}$$

$$\alpha_3 = \varepsilon_b^2 h = \frac{1}{2}\varepsilon_b h_1 + \frac{1}{16}h_2 - H\left[\varepsilon_b^2 h^2 - \frac{1}{2}\varepsilon_b h h_1 + \frac{1}{16}h_1^2\right]. \tag{C5c}$$

In Eqs. (C5a)–(C5c), H is a short-hand notation for $(\omega-\varepsilon_b)/[1+(\omega-\varepsilon_b)h(\omega)]$. The method developed in Appendix A to calculate $\underline{u}^+ \mathbf{B_2} \underline{u}$ is applicable also for the triangular lattice up to Eq. (A17) which yields the optimum spin-flip energy for RES3.

The elements of the 2×2 matrices $\mathbf{A}$ and $\mathbf{B}$ are given by $a_1 = \alpha_1 - (\omega - \varepsilon_b - U)$, $a_2 = \alpha_3$, $a_3 = \alpha_2$, $b_1 = \overline{h}(\omega)$, $b_2 = \overline{h_2}(\omega)/\varepsilon_b^2$, $b_3 = \overline{h_1}(\omega)/\varepsilon_b$ with $\overline{h_1}(\omega)$ and $\overline{h_2}(\omega)$ defined in analogy to Eq. (C2) as integrals over the Fermi sphere.

APPENDIX D: KAGOMÉ LATTICE

To prepare the derivation of the ansatzes RES0–RES3 for the frustrated *kagomé* lattice we diagonalize the one-particle problem explicitly. Since we deal with a non-Bravais lattice with three sites per unit cell we have to solve a 3×3 eigenvalue problem with

$$f_{\alpha,\underline{j}} = \exp(i\underline{\underline{k}}\,\underline{j})\,\phi_{\alpha,\tau(\underline{j})}, \tag{D1}$$

where $\tau(j) \in \{1,2,3\}$ denotes the sublattice to which site $\underline{j}$ belongs. The one-particle Hamiltonian acting on $\phi_{\alpha,\tau}$ becomes

$$h(\underline{k}) = 2t \times \begin{bmatrix} 0 & \cos(\underline{\underline{k}}\,\underline{n}_1/2) & \cos\left(\dfrac{\underline{\underline{k}}\,\underline{n}_2}{2}\right) \\ \cos\left(\dfrac{\underline{\underline{k}}\,\underline{n}_1}{2}\right) & 0 & \cos\left(\dfrac{\underline{\underline{k}}(\underline{n}_2-\underline{n}_1)}{2}\right) \\ \cos\left(\dfrac{\underline{\underline{k}}\,\underline{n}_2}{2}\right) & \cos\left(\dfrac{\underline{\underline{k}}(\underline{n}_2-\underline{n}_1)}{2}\right) & 0 \end{bmatrix}, \tag{D2}$$

where we used the unit vectors $\underline{n}_1$ and $\underline{n}_2$ as shown in Fig. 18. The secular equation of Eq. (D2) is

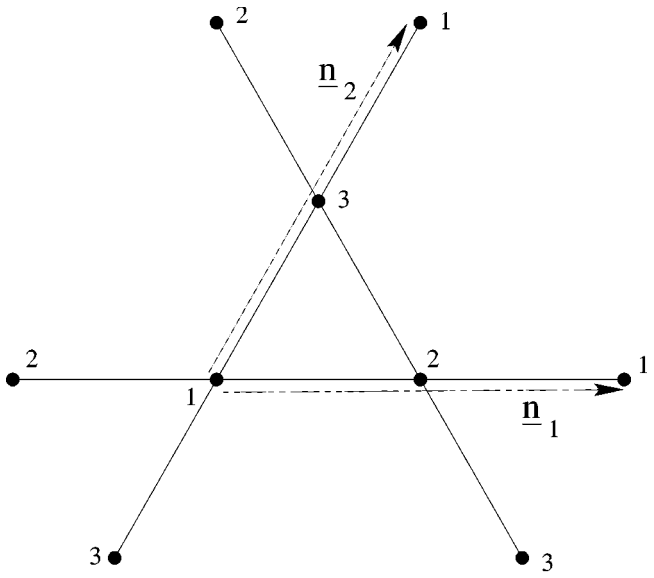

FIG. 18. Segment of the *kagomé* lattice. The vectors are used in the main text. The numbers refer to the three sites in each unit cell of this non-Bravais lattice.

$$0=(-2t+\lambda)[\lambda^2+2t\lambda-2t^2+t\varepsilon_{\triangle}(\underline{k})], \tag{D3}$$

where $\varepsilon_{\triangle}(\underline{k})$ is the triangular dispersion (44). From the secular equation one deduces Eq. (45) easily. More important for the following is the observation that $h(\underline{k})$ can be diagonalized by an orthogonal, i.e., real, transformation since it is real symmetric. Thus the phase of $f_{\alpha,\underline{j}}$ is completely given by the plane-wave factor $\exp(i\underline{k}\underline{j})$ in Eq. (D1).

Since we wish to treat the frustrated case ($t<0$) we modify the ansatz (B6) by introducing an additional phase factor $\lambda_{\underline{j}}$ depending only on the sublattice and being unity on sublattice 1, $\exp(2\pi i/3)$ on sublattice 2, and $\exp(-2\pi i/3)$ on sublattice 3

$$\Phi_\alpha:=\sum_{\underline{j}} a_{\underline{j}\uparrow}c^+_{\alpha\uparrow}a^+_{\underline{j}\downarrow}|\mathcal{N}\!\!\!/\rangle f^+_{\alpha,\underline{j}}\lambda^+_{\underline{j}}. \tag{D4}$$

The resulting matrix elements $\mathbf{P}_{\alpha\!\!\!/,\alpha}$ and $\mathbf{L}_{\uparrow\alpha\!\!\!/,\alpha}$ are the same as in Eqs. (B7a,B7b) since the phase factor cancels at each site. But $\mathbf{L}_{\downarrow\alpha\!\!\!/,\alpha}$ does change into

$$\mathbf{L}_{\downarrow\alpha\!\!\!/,\alpha}=\frac{e_1\varepsilon_\alpha}{2zt}\delta_{\alpha\!\!\!/,\alpha}-t\sum_{\langle\underline{i},\underline{j}\rangle}|f_{\alpha\!\!\!/,\underline{i}}|^2|f_{\alpha,\underline{j}}|^2\lambda^+_{\underline{i}}\lambda_{\underline{j}}. \tag{D5}$$

The change in the second term is obvious. The change in the first term A_1 is less trivial. In a first step one obtains

$$A_1=-\frac{e_1}{zt}\delta_{\alpha\!\!\!/,\alpha}\sum_{\underline{k},\underline{\delta}} f^+_{\alpha,\underline{j}}f_{\alpha,\underline{j}+\underline{\delta}}\lambda^+_{\underline{j}}\lambda_{\underline{j}+\underline{\delta}}. \tag{D6}$$

Transforming the terms of the sum like $\underline{\delta}\to-\underline{\delta}$ and $\underline{j}\to\underline{j}+\underline{\delta}$ leads to

$$f^+_{\alpha,\underline{j}}f_{\alpha,\underline{j}+\underline{\delta}}\lambda^+_{\underline{j}}\lambda_{\underline{j}+\underline{\delta}}\to f^+_{\alpha,\underline{j}+\underline{\delta}}f_{\alpha,\underline{j}+2\underline{\delta}}\lambda_{\underline{j}}\lambda^+_{\underline{j}+\underline{\delta}}$$
$$=f^+_{\alpha,\underline{j}}f_{\alpha,\underline{j}+\underline{\delta}}\lambda_{\underline{j}}\lambda^+_{\underline{j}+\underline{\delta}}. \tag{D7}$$

The last equality holds since $\phi_{\alpha,\tau(\underline{j})}$ in Eq. (D1) is real. Hence only the real part of $\lambda^+_{\underline{j}}\lambda_{\underline{j}+\underline{\delta}}$ in Eq. (D6) matters. It is $-1/2$ leading thus to the first term in Eq. (D5).

From the matrix elements (B7a),(B7b),(D5) we find the relations which are analogous to Eqs. (B8b),(B8c),(B9a),(B9b)

$$\mathbf{D}_{\alpha\!\!\!/,\alpha}=\delta_{\alpha\!\!\!/,\alpha}[n(\omega-\varepsilon_\alpha)+e_1-(e_1/2zt)\varepsilon_\alpha]^{-1}, \tag{D8a}$$

$$\mathbf{N}_{\alpha\!\!\!/,\alpha}=\omega\sum_{\underline{j}}|f_{\alpha\!\!\!/,\underline{j}}|^2|f_{\alpha,\underline{j}}|^2+t\sum_{\langle\underline{i},\underline{j}\rangle}|f_{\alpha\!\!\!/,\underline{i}}|^2|f_{\alpha,\underline{j}}|^2\lambda^+_{\underline{i}}\lambda_{\underline{j}}, \tag{D8b}$$

$$\mathbf{M}_{\underline{i},\underline{j}}:=\sum_\alpha\frac{|f_{\alpha,\underline{i}}|^2|f_{\alpha,\underline{j}}|^2}{n(\omega-\varepsilon_\alpha)+e_1-(e_1/2zt)\varepsilon_\alpha}, \tag{D8c}$$

$$\mathbf{A}_{\underline{i},\underline{j}}:=\omega\delta_{\underline{i},\underline{j}}+t\sum_{\underline{\delta}}\delta_{\underline{i}+\underline{\delta},\underline{j}}\lambda^+_{\underline{i}}\lambda_{\underline{j}}. \tag{D8d}$$

The vector $\underline{u}$ is again an eigenvector of the matrices $\mathbf{M}$ and $\mathbf{A}$. Its eigenvalue for $\mathbf{M}$ is in analogy to Eq. (B11) identical to Eq. (16a) with the adapted definition

$$\gamma_{\mathrm{K}}=n+e_1/(2zt). \tag{D9}$$

The eigenvalue for $\mathbf{A}$ is $\omega-zt/2=\omega-\varepsilon_{\mathrm{b}}$ as before. So the series in Eq. (B10) yields a vanishing denominator for $0=1+(\omega-\varepsilon_{\mathrm{b}})h(\omega)$ with $h(\omega)$ as in Eq. (16a) with γ [Eq. (16c)] replaced by γ_{K} [Eq. (D9)]. So the DOS, the lower band edge ε_{b}, and γ_{K} are the only quantities to be changed so that RES0 (15) applies to the frustrated *kagomé* lattice.

For RES1 the ansatz reads

$$|\Psi_1\rangle:=|\Lambda|^{-1/2}\sum_{\underline{i}}\exp(i\underline{k}_{\mathrm{b}}\underline{i})a^+_{\underline{i}\uparrow}a_{\underline{i}\uparrow}a^+_{\underline{i}\downarrow}|\mathcal{N}\!\!\!/\rangle\lambda^+_{\underline{i}} \tag{D10}$$

in extension of Eq. (18). The resulting condition is identical to Eq. (23) with the adapted γ_{K} in Eq. (D9) and, of course, $\varepsilon_{\mathrm{b}}=zt/2$.

For RES2 the ansatz reads

$$|\Psi_2\rangle:=|\Lambda|^{-1/2}\sum_{\langle\underline{i}\underline{j}\rangle}\exp(i\underline{k}_{\mathrm{b}}\underline{i})a^+_{\underline{i}\uparrow}a_{\underline{j}\uparrow}a^+_{\underline{i}\downarrow}|\mathcal{N}\!\!\!/\rangle\lambda^+_{\underline{i}} \tag{D11}$$

yielding again condition (28) with the adapted quantities, in particular $\gamma_{\mathrm{K}}\!\!\!/:=e_1+e_2/(2zt)$.

The ansatz for the doubly occupied states in RES3 is the extension of Eq. (B14)

$$\Psi_\beta=\sum_{\underline{j}}a^+_{\underline{j}\uparrow}c_{\beta\uparrow}a^+_{\underline{j}\downarrow}|\mathcal{N}\!\!\!/\rangle f_{\beta,\underline{j}}\lambda^+_{\underline{j}}. \tag{D12}$$

The relations analogous to Eqs. (B15a),(B15b),(B16),(B17c) read

$$(\mathbf{D_1})_{\alpha\underline{\beta},\alpha}=\delta_{\alpha\underline{\beta},\alpha}[n(\omega-\varepsilon_\alpha)+e_1-e_1\varepsilon_\alpha/(2zt)] + \omega\sum_{\underline{j}} |f_{\alpha\underline{\beta},\underline{j}}|^2|f_{\alpha,\underline{j}}|^2+t\sum_{\langle\underline{i},\underline{j}\rangle} |f_{\alpha\underline{\beta},\underline{i}}|^2|f_{\alpha,\underline{j}}|^2\lambda_{\underline{i}}^{+}\lambda_{\underline{j}}, \tag{D13a}$$

$$(\mathbf{D_2})_{\beta\underline{\beta},\beta}=\delta_{\beta\underline{\beta},\beta}[\delta(\omega-U+\varepsilon_\beta)+e_1+e_1\varepsilon_\beta/(2zt)] + \omega\sum_{\underline{j}} |f_{\beta\underline{\beta},\underline{j}}|^2|f_{\beta,\underline{j}}|^2+t\sum_{\langle\underline{i},\underline{j}\rangle} |f_{\beta\underline{\beta},\underline{i}}|^2|f_{\beta,\underline{j}}|^2\lambda_{\underline{i}}^{+}\lambda_{\underline{j}}, \tag{D13b}$$

$$\mathbf{N}_{\alpha,\beta}=t\sum_{\underline{i},\underline{j}} (f_{\alpha,\underline{j}}^{+}f_{\alpha,\underline{i}}|f_{\beta,\underline{i}}|^2-|f_{\alpha,\underline{i}}|^2f_{\beta,\underline{j}}^{+}f_{\beta,\underline{i}}) + t\sum_{\underline{i},\underline{j}}\left(\frac{-1}{2}f_{\alpha,\underline{i}}^{+}f_{\alpha,\underline{j}}f_{\beta,\underline{j}}^{+}f_{\beta,\underline{i}}-|f_{\alpha,\underline{j}}|^2|f_{\beta,\underline{i}}|^2\lambda_{\underline{i}}^{+}\lambda_{\underline{j}}\right), \tag{D13c}$$

$$\mathbf{E}_{\underline{i},\underline{\delta}\underline{\beta};\underline{j},\underline{\delta}}=-t\delta_{\underline{i},\underline{j}}(\delta_{\underline{\delta}\underline{\beta},0}-\delta_{\underline{\delta},0})-\frac{t}{2}\delta_{\underline{i}-\underline{\delta}\underline{\beta},\underline{j}}\delta_{\underline{\delta},-\underline{\delta}\underline{\beta}}(1-\delta_{\underline{\delta},0}) -t\sum_{\underline{\delta}\underline{\beta}} \delta_{\underline{i}+\underline{\delta}\underline{\beta},\underline{j}}\delta_{\underline{\delta}\underline{\beta},0}\delta_{\underline{\delta},0}\lambda_{\underline{i}}^{+}\lambda_{\underline{j}}. \tag{D13d}$$

So far the analogy to the treatment of unfrustrated lattices is perfect once the different form of ε_b, γ_K, and of $\overline{\gamma_K}=\delta+e_1/(2zt)$ is taken into account. In particular the formulas (B21),(B24) for the matrices $\mathbf{C_1}$ and $\mathbf{C_2}$ carry over. But due to the different form of Eq. (D13d) the matrix $\mathbf{E}$ is changed compared to Eq. (B19)

$$\mathbf{E}\underline{u}=zt/2\underline{u}+\sqrt{z}t\underline{v}, \tag{D14a}$$

$$\mathbf{E}\underline{v}=-\sqrt{z}t\underline{u}-t/2\underline{v}, \tag{D14b}$$

$$\Rightarrow\tilde{\mathbf{E}}=t\begin{bmatrix} z/2 & -\sqrt{z} \\ \sqrt{z} & -1/2 \end{bmatrix} \tag{D14c}$$

acting on $(\underline{u},\underline{v})$. This matrix is no longer singular as was $\mathbf{E}$ in Eq. (B20). Thus we stay on the 2×2 matrix level. The singularity condition based on Eq. (B18) is

$$0=\det(1-\mathbf{C_2}\tilde{\mathbf{E}}^{+}\mathbf{C_1}\tilde{\mathbf{E}}), \tag{D15}$$

which can be evaluated easily. This concludes the derivation for the RES3 ansatz on the frustrated *kagomé* lattice.

APPENDIX E: DOS FOR THE LATTICES CONSIDERED

In this appendix we give the explicit formulas for the densities of states for the lattices discussed in Sec. III. $K[m]$ stands for the complete elliptic integral of the first kind (see, e.g., Ref. 49).

Square lattice

$$\rho_{\square}(\varepsilon)=(2|t|\pi^2)^{-1}\cdot K\left[1-\left(\frac{\varepsilon}{4t}\right)^2\right]. \tag{E1}$$

Simple cubic lattice

$$\rho_{sc}(\varepsilon)=\pi^{-1}\int_{u_1}^{u_2}\frac{du}{\sqrt{1-u^2}}\cdot\rho_{\square}(\varepsilon+2tu), \tag{E2a}$$

$$u_1=\max(-1,-2-\varepsilon/(2t)), \tag{E2b}$$

$$u_2=\min(1,2-\varepsilon/(2t)). \tag{E2c}$$

bcc lattice

$$\rho_{bcc}(\varepsilon)=\frac{2}{\pi}\int_{|\varepsilon|/2}^{4|t|}\frac{du}{\sqrt{4u^2-\varepsilon^2}}\cdot\rho_{\square}(u). \tag{E3}$$

Triangular lattice

$$\rho_{\triangle}(\varepsilon)=(\sqrt{z_0}t\pi^2)^{-1}\cdot K[z_1/z_0]. \tag{E4a}$$

For $t>0$, z_0 and z_1 are given by

$$z_0=\begin{cases} 3+2\sqrt{3-\varepsilon/t}-(\varepsilon/(2t))^2 & \text{for } 2t\leq\varepsilon\leq3t \\ 4\sqrt{3-\varepsilon/t} & \text{for } -6t\leq\varepsilon\leq2t, \end{cases} \tag{E4b}$$

$$z_1=\begin{cases} 4\sqrt{3-\varepsilon/t} & \text{for } 2t\leq\varepsilon\leq3t \\ 3+2\sqrt{3-\varepsilon/t}-(\varepsilon/(2t))^2 & \text{for } -6t\leq\varepsilon\leq2t. \end{cases} \tag{E4c}$$

For $t<0$, the upper and lower intervals in Eqs. (E4b) and (E4c) have to be replaced by $-3|t|\leq\varepsilon\leq-2|t|$ and $-2|t|\leq\varepsilon\leq6|t|$, respectively.

Honeycomb lattice

$$\rho_H(\varepsilon)=|\varepsilon/t|\cdot\rho_{\triangle}(3t-\varepsilon^2/t). \tag{E5}$$

Kagomé lattice

$$\rho_K(\varepsilon)=\frac{1}{3}\delta(\varepsilon-2t)+\frac{2}{3}|1+\varepsilon/t|\cdot\rho_{\triangle}(3t-(\varepsilon+t)^2/t). \tag{E6}$$

Hcp lattice ($t=-1$)

$$\rho_{hcp}(\varepsilon)=\frac{2}{\pi}\int_0^1 dy\,\Xi(y), \tag{E7a}$$

with the integrand

$$\Xi(y)=\begin{cases} \sqrt{-2-\varepsilon_-}\dfrac{\rho_{\triangle}[\varepsilon_--(2+\varepsilon_-)y^2]}{\sqrt{\varepsilon_+-\varepsilon_-+(2+\varepsilon_-)y^2}} \\ +\sqrt{2+\varepsilon_+}\dfrac{\rho_{\triangle}[\varepsilon_+-(2+\varepsilon_+)y^2]}{\varepsilon_+-(2+\varepsilon_+)y^2-\varepsilon_-} & \text{for } \varepsilon\leq0, \\ \sqrt{6-\varepsilon_-}\dfrac{\rho_{\triangle}[\varepsilon_-+(6-\varepsilon_-)y^2]}{\sqrt{\varepsilon_+-\varepsilon_--(6-\varepsilon_-)y^2}} & \text{for } \varepsilon\geq0 \end{cases} \tag{E7b}$$

and

$$\varepsilon_{\pm}=\varepsilon+2(1\pm\sqrt{\varepsilon+4}). \tag{E7c}$$

[1] M. C. Gutzwiller, Phys. Rev. Lett. **10**, 159 (1963).
[2] J. Hubbard, Proc. R. Soc. London **276**, 238 (1963).
[3] J. Kanamori, Prog. Theor. Phys. **30**, 275 (1963).
[4] A. Mielke and H. Tasaki, Commun. Math. Phys. **158**, 341 (1993).
[5] M. Kollar, R. Strack, and D. Vollhardt, Phys. Rev. B **53**, 9225 (1996).
[6] P. Fazekas, cond-mat/9612090 (unpublished).
[7] D. Vollhardt *et al.*, Z. Phys. B **103**, 283 (1997).
[8] E. Müller-Hartmann, J. Low Temp. Phys. **99**, 349 (1995).
[9] K. Penc, H. Shiba, F. Mila, and T. Tsukagoshi, Phys. Rev. B **54**, 4056 (1996).
[10] P. Pieri *et al.*, Phys. Rev. B **54**, 9250 (1996).
[11] S. Daul and R. M. Noack, Z. Phys. B **103**, 293 (1997).
[12] P. A. Sreeram and S. G. Mishra, cond-mat/9703022 (unpublished).
[13] G. S. Uhrig, Phys. Rev. Lett. **77**, 3629 (1996).
[14] M. Ulmke, cond-mat/9512044; cond-mat/9704229 (unpublished).
[15] R. Hlubina, S. Sorella, and F. Guinea, Phys. Rev. Lett. **78**, 1343 (1997).
[16] T. Herrmann and W. Nolting, J. Magn. Magn. Mater. **170**, 253 (1997).
[17] T. Herrmann and W. Nolting, Solid State Commun. **103**, 351 (1997).
[18] Y. Nagaoka, Solid State Commun. **3**, 409 (1965).
[19] H. Tasaki, Phys. Rev. B **40**, 9192 (1989).
[20] A. Barbieri, J. A. Riera, and A. P. Young, Phys. Rev. B **41**, 11 697 (1990).
[21] G.-S. Tian, Phys. Rev. B **44**, 4444 (1991).
[22] M. Takahashi, Prog. Theor. Phys. **42**, 1098 (1992).
[23] P. Wurth, G. S. Uhrig, and E. Müller-Hartmann, Ann. Phys. (Leipzig) **5**, 148 (1996).
[24] T. Hanisch and E. Müller-Hartmann, Ann. Phys. (Leipzig) **2**, 381 (1993).
[25] T. Hanisch, B. Kleine, A. Ritzl, and E. Müller-Hartmann, Ann. Phys. (Leipzig) **4**, 303 (1995).
[26] T. Okabe, Prog. Theor. Phys. **97**, 21 (1997).
[27] W. F. Brinkman and T. M. Rice, Phys. Rev. B **2**, 1324 (1970).
[28] B. S. Shastry, H. R. Krishnamurthy, and P. W. Anderson, Phys. Rev. B **41**, 2375 (1990).
[29] E. Müller-Hartmann, in *Proceedings of the V. Symposium ''Physics of Metals,''* edited by E. Talik and J. Szade (Symposium ''Physics of Metals,'' Ustron-Jaszowiec, Poland, 1991), p. 22.
[30] E. Müller-Hartmann, T. Hanisch, and R. Hirsch, Physica B **186-188**, 834 (1993).
[31] A. G. Basile and V. Elser, Phys. Rev. B **41**, 4842 (1990).
[32] G. S. Uhrig, Phys. Rev. B **54**, 10 436 (1996).
[33] P. Fulde, *Electron Correlations in Molecules and Solids*, Vol. 100 of *Solid State Sciences* (Springer-Verlag, Berlin, 1993).
[34] M. C. Gutzwiller, Phys. Rev. **137**, 1726 (1963).
[35] F. Gebhard and X. Zotos, Phys. Rev. B **43**, 1176 (1991).
[36] W. von der Linden and D. M. Edwards, J. Phys.: Condens. Matter **3**, 4917 (1991).
[37] P. Wurth and E. Müller-Hartmann, Ann. Phys. (Leipzig) **4**, 144 (1995).
[38] L. Roth, Phys. Rev. **186**, 428 (1969).
[39] B. W. Tan, Ph.D. thesis, Imperial College, 1974.
[40] S. R. Allan and D. M. Edwards, J. Phys. F **12**, 1203 (1982).
[41] P. Fazekas, B. Menge, and E. Müller-Hartmann, Z. Phys. B **78**, 69 (1990).
[42] The line graph of a graph (lattice) is constructed by converting edges into vertices. Two vertices of the line graph are linked if the corresponding edges on the original graph had a vertex in common.
[43] A. Mielke, J. Phys. A **24**, L73 (1991); **24**, 3311 (1991).
[44] A. Mielke, J. Phys. A **25**, 4335 (1991); **174**, 443 (1993).
[45] H. Tasaki, Phys. Rev. Lett. **75**, 4678 (1995).
[46] W. Metzner and D. Vollhardt, Phys. Rev. Lett. **62**, 324 (1989).
[47] N. D. Mermin and H. Wagner, Phys. Rev. Lett. **17**, 1133 (1966).
[48] E. N. Economou, *Green's Functions in Quantum Physics*, Vol. 7 of *Solid State Sciences* (Springer, Berlin, 1979).
[49] M. Abramowitz and I. A. Stegun, *Handbook of Mathematical Functions* (Dover, New York, 1964).